ARTICLE IN PRESS

Computers and Mathematics with Applications ▮ (▮▮▮▮) ▮▮▮–▮▮▮

Contents lists available at ScienceDirect

Computers and Mathematics with Applications

journal homepage: www.elsevier.com/locate/camwa

Modeling of first-order photobleaching kinetics using Krylov subspace spectral methods

Somayyeh Sheikholeslami [a], James V. Lambers [b,*]

[a] The University of Southern Mississippi, Department of Physics and Astronomy, Hattiesburg, MS, 39406, USA
[b] The University of Southern Mississippi, Department of Mathematics, Hattiesburg, MS, 39406, USA

ARTICLE INFO

Article history:
Available online xxxx

Keywords:
Lanczos algorithm
Spectral methods
Gaussian quadrature
FRAP
Photobleaching kinetics equation

ABSTRACT

We solve the first order 2-D reaction–diffusion equations which describe binding-diffusion kinetics using the photobleaching scanning profile of a confocal laser scanning microscope, approximated by a Gaussian laser profile. We show how to solve the first-order photobleaching kinetics partial differential equations (PDEs) using a time-stepping method known as a Krylov subspace spectral (KSS) method. KSS methods are explicit methods for solving time-dependent variable-coefficient partial differential equations. They approximate Fourier coefficients of the solution using Gaussian quadrature rules in the spectral domain. In this paper, we show how a KSS method can be used to obtain not only an approximate numerical solution, but also an approximate analytical solution when using initial conditions that come from pre-bleach steady states and also general initial conditions, to facilitate asymptotic analysis. Analytical and numerical results are presented. It is observed that although KSS methods are explicit, it is possible to use a time step that is far greater than what the CFL condition would indicate.

1. Introduction

Fluorescence recovery after photobleaching (FRAP) is a method used to obtain information about the dynamic behavior of the molecules in a cell membrane. A high-intensity laser beam is used to bleach molecules in a region of the cell. The redistribution of the molecules is monitored in both bleached and unbleached regions over time to investigate the movements of molecules within membrane domains. The FRAP method was established by Jacobson et al. in 1976 [1]. The chemical equation of the binding-diffusion process that happens in FRAP is

$$u + a \underset{k_{\text{off}}}{\overset{k_{\text{on}}}{\rightleftharpoons}} b, \tag{1}$$

where u denotes unbound molecules, a refers to specific binding sites, and b represents bound complexes (ua). The rate of the forward binding reaction is called k_{on}, where a molecule binds to a binding site to form a bound complex, and k_{off} refers to the rate of the reverse unbinding reaction where a molecule is released from its binding site. The first-order reaction–diffusion equations which describe binding-diffusion kinetics are

$$\frac{\partial u}{\partial t} = -k_b I_{r_n}(x, y)u + D_1 \Delta u - k_{\text{on}} u + k_{\text{off}} b$$

* Corresponding author.
E-mail address: James.Lambers@usm.edu (J.V. Lambers).

https://doi.org/10.1016/j.camwa.2017.10.019
0898-1221/

$$\frac{\partial b}{\partial t} = -k_b I_{r_n}(x,y)b + D_2 \Delta b + k_{\text{on}} u - k_{\text{off}} b \tag{2}$$
$$\Delta = \frac{\partial^2}{\partial x^2} + \frac{\partial^2}{\partial y^2}, \quad D_1 > D_2$$

where the initial conditions from the pre-bleach steady state are

$$u(x,y,0) = \frac{k_{\text{off}}}{k_{\text{on}} + k_{\text{off}}} c_i \tag{3}$$
$$b(x,y,0) = \frac{k_{\text{on}}}{k_{\text{on}} + k_{\text{off}}} c_i. \tag{4}$$

D_1 and D_2 are diffusion coefficients of u and b, respectively; k_{on} and k_{off} are the on and off binding-rate constants, k_b is a bleach constant which is the intensity of the bleaching laser, determined from the properties of the fluorophore, and c_i is the initial concentration of the fluorescent molecules inside the bleached zone. Also, D_1, D_2, k_{on} and k_{off} are positive constants. The photobleaching scanning profile of the confocal of the Gaussian laser can be approximated by [2–4]

$$I_{r_n}(x,y) = \frac{2I_0}{\pi r_n^2} e^{-\frac{2((x-x_c)^2+(y-y_c)^2)}{r_n^2}}$$

where r_n is the nominal radius of the laser beam and (x_c, y_c) is the center.

First-order photobleaching kinetics which are mathematically modeled in Eq. (2) were solved numerically by Kang et al. [4,5]. These equations were also solved numerically using an inversion method (methods of lines, with backward Euler in time and central differencing in space) in [6]. In this paper we apply an explicit time-stepping method known as a Krylov subspace spectral (KSS) method to solve the first-order photobleaching kinetics PDEs. KSS methods developed by Lambers [7] use Gaussian quadrature rules in the spectral domain, as described in [8], to approximate each Fourier coefficient of the solution. This component-wise approach yields high-order accuracy in time, stability characteristic of implicit methods even though KSS methods are themselves explicit [7,9], and superior scalability compared to other time-stepping approaches [10]. We will use a KSS method to solve the first-order photobleaching kinetics equations with initial conditions (3), (4). By applying KSS symbolically to compute each Fourier coefficient, we can also obtain an approximate analytical solution valid for a sufficiently small time step, to facilitate qualitative analysis of the solution.

The outline of the paper is as follows. In Section 2, we describe KSS methods. In Section 3 we use a first-order KSS method to derive formulas for the Fourier coefficients of an approximate solution with general initial data. In Section 4 we derive formulas for the Fourier coefficients of an approximate analytical solution, for sufficiently small time, with initial data obtained from pre-bleach steady states. In Section 5 we explain how this KSS method can be implemented efficiently. Section 6 presents numerical results to validate our approximate analytical solution and demonstrate the accuracy and efficiency of the corresponding numerical method, and Section 7 gives concluding remarks and discussion of future work, including generalizations.

2. Methodology

2.1. Krylov subspace spectral methods

In order to solve Eq. (2), we apply a Krylov subspace spectral (KSS) method [7] in $[0, 2\pi]^2$ and $t > 0$ with periodic boundary conditions. To describe KSS methods, we scale down to a simpler problem, a single 1-D PDE on $[0, 2\pi]$ rather than a system of two 2-D PDEs:

$$\frac{\partial u}{\partial t} + L(x,D)u = 0, \qquad u(x,0) = u_0(x)$$
$$u(0,t) = u(2\pi, t)$$

where $D = \partial/\partial x$ and $L(x, D)$ is a differential operator which includes both differentiation operators and coefficients that are functions of x. The inner product $\langle \cdot, \cdot \rangle$ is the standard L^2 inner product of functions on $[0, 2\pi]$. The Fourier coefficients of the exact solution as inner products are calculated as follows:

$$\langle f, g \rangle = \int_0^{2\pi} \overline{f(x)} g(x)\, dx$$
$$\hat{u}(\omega, t_{n+1}) = \left\langle \frac{1}{\sqrt{2\pi}} e^{i\omega x}, S(x, D; \Delta t) u(x, t_n) \right\rangle, \quad |\omega| \le N/2 \tag{5}$$

where $S(x, D; \Delta t) = e^{-L(x,D)\Delta t}$ is the exact solution operator and N is the number of equally-spaced grid points. After spatial discretization, (5) becomes

$$[\hat{u}^{n+1}]_\omega = \hat{e}_\omega^H S_N(\Delta t) u(t_n), \quad S_N = e^{-L_N \Delta t} \tag{6}$$

Please cite this article in press as: S. Sheikholeslami, J.V. Lambers, Modeling of first-order photobleaching kinetics using Krylov subspace spectral methods, Computers and Mathematics with Applications (2017), https://doi.org/10.1016/j.camwa.2017.10.019.

where L_N is a matrix that represents the spatial discretization of the operator $L(x, D)$. Vector components on a N-point grid and uniform grid spacing h are defined by

$$\left[\hat{e}_\omega\right]_j = \frac{1}{\sqrt{2\pi}} e^{i\omega jh}, \qquad [u(t_n)]_j = u(jh, t_n), \qquad h = \frac{2\pi}{N}.$$

2.2. Gaussian quadrature for Riemann–Stieltjes integrals

The bilinear form in Eq. (6) that we want to approximate is an example of the generic bilinear form

$$\mathbf{u}^H f(A)\mathbf{v} \tag{7}$$

where $\mathbf{u}$ and $\mathbf{v}$ are N-vectors, f is a smooth function and $A = L_N$ is an $N \times N$ symmetric positive definite matrix with positive and real eigenvalues

$$0 < a = \lambda_N \leq \cdots \leq \lambda_2 \leq \lambda_1 = b \tag{8}$$

and also orthonormal eigenvectors $\mathbf{q}_1, \mathbf{q}_2, \ldots, \mathbf{q}_N$ such that

$$A\mathbf{q}_j = \lambda_j \mathbf{q}_j, \quad j = 1, 2, \ldots, N. \tag{9}$$

As shown in [8], the bilinear form (7) can be written as Riemann–Stieltjes integral

$$\begin{aligned}\mathbf{u}^H f(A)\mathbf{v} &= \mathbf{u}^H f\left(\sum_{j=1}^{N} \lambda_j \mathbf{q}_j \mathbf{q}_j^H\right)\mathbf{v} \\ &= \sum_{j=1}^{N} f(\lambda_j)\mathbf{u}^H \mathbf{q}_j \mathbf{q}_j^H \mathbf{v} \\ &= \int_a^b f(\lambda)\, d\alpha(\lambda).\end{aligned}$$

The measure $\alpha(\lambda)$ is defined as

$$\alpha(\lambda) = \begin{cases} 0, & \lambda < a \\ \displaystyle\sum_{j=i}^{N} \alpha_j \beta_j, & \lambda_i \leq \lambda < \lambda_{i-1}, \quad i = 1, \ldots, N-1 \\ \displaystyle\sum_{j=1}^{N} \alpha_j \beta_j, & b \leq \lambda \end{cases} \tag{10}$$

where $\alpha_j = \mathbf{u}^H \mathbf{q}_j$ and $\beta_j = \mathbf{q}_j^H \mathbf{v}$. A K-node Gaussian quadrature rule can be written in terms of nodes t_j and weights w_j where $j = 1, 2, \ldots, K$.

$$\mathbf{u}^H f(A)\mathbf{v} = \int_a^b f(\lambda)\, d\alpha(\lambda) = I[f] = \sum_{j=1}^{K} w_j f(t_j) + R[f].$$

The weights are calculated by

$$w_j = \int_a^b L_j(\lambda) d\alpha(\lambda), \quad j = 1, 2, \ldots, K,$$

where $L_j(\lambda)$ is a Lagrange polynomial for the nodes $t_1, \ldots, t_K$ that can be written

$$\begin{aligned} L_j(\lambda) &= \prod_{i=1, i\neq j}^{K} \frac{\lambda - t_i}{\lambda_j - \lambda_i}, \quad j = 1, \ldots, K \\ L_j(t_k) &= \delta_{jk}. \end{aligned}$$

The error can be calculated by

$$R[f] = \frac{f^{2K}(\eta)}{(2K)!} \int_a^b \left[\prod_{j=1}^{K} (\lambda - t_j)\right]^2 d\alpha(\lambda), \quad a < \eta < b.$$

Please cite this article in press as: S. Sheikholeslami, J.V. Lambers, Modeling of first-order photobleaching kinetics using Krylov subspace spectral methods, Computers and Mathematics with Applications (2017), https://doi.org/10.1016/j.camwa.2017.10.019.

2.3. The case $\mathbf{u} = \mathbf{v}$

In order to construct a Gaussian quadrature rule for the measure $\alpha(\lambda)$, we define a sequence of polynomials $q_0(\lambda)$, $q_1(\lambda)$, ... that are orthonormal. Orthonormality is defined by the conditions

$$\int_a^b q_i(\lambda) q_j(\lambda)\, d\alpha(\lambda) = \delta_{ij}$$

where q_j has exact degree j for $j = 0, 1, 2, \ldots$. We therefore use the inner product we could write

$$\langle f, g\rangle = \int_a^b \overline{f(\lambda)} g(\lambda)\, d\alpha(\lambda) = \mathbf{u}^H f(A) g(A) \mathbf{v}.$$

The polynomials $q_0, q_1, \ldots$ satisfy a three-term recurrence relationship, which, for $j = 1, 2, \ldots$, can be written

$$\beta_j q_j(\lambda) = (\lambda - \alpha_j) q_{j-1}(\lambda) - \beta_{j-1} q_{j-2}(\lambda), \quad q_{-1}(\lambda) \equiv 0, \quad q_0(\lambda) \equiv \left(\int_a^b d\alpha(\lambda) \right)^{-1/2},$$

where for $j = 1, 2, \ldots, K$ we have

$$\begin{aligned}
\alpha_j &= \langle q_{j-1}, x q_{j-1}\rangle = \mathbf{x}_j^H A \mathbf{x}_j, \quad j \geq 1 \\
\beta_j &= \langle p_j, p_j\rangle^{1/2} = \|\mathbf{r}_j\|_2 \\
\mathbf{x}_j &= q_{j-1}(A)\mathbf{u}, \quad j \geq 1 \\
\mathbf{r}_j &= p_j(A)\mathbf{u} = (A - \alpha_j I) q_{j-1}(A)\mathbf{u} - \beta_{j-1} q_{j-2}(A)\mathbf{u} = \\
&\quad (A - \alpha_j I)\mathbf{x}_j - \beta_{j-1}\mathbf{x}_{j-1}
\end{aligned}$$

where α_j and β_j are recursion coefficients, and $\mathbf{x}_j$ and $\mathbf{r}_j$ are vectors. The resulting orthonormal polynomials and tridiagonal Jacobi matrix J_K, produced by Lanczos iteration, are

$$\mathbf{q}(\lambda) = \begin{bmatrix} q_0(\lambda) \\ q_1(\lambda) \\ \vdots \\ q_{K-1}(\lambda) \end{bmatrix}, \quad J_K = \begin{bmatrix} \alpha_1 & \beta_1 & & & \\ \beta_1 & \alpha_2 & \beta_2 & & \\ & \ddots & \ddots & \ddots & \\ & & \beta_{K-2} & \alpha_{K-1} & \beta_{K-1} \\ & & & \beta_{K-1} & \alpha_K \end{bmatrix}. \tag{11}$$

The eigenvalues of J_K are the nodes for a K-point Gaussian quadrature rule. The squares of the first elements of the normalized eigenvectors of J_K are the weights $w_j = (\beta_0 q_0(t_j)/\|\mathbf{q}(t_j)\|_2)^2$. We then have the Gaussian quadrature approximation

$$\mathbf{u}^H f(A)\mathbf{u} = \|\mathbf{u}\|_2^2 \mathbf{e}_1^H f(J_K)\mathbf{e}_1,$$

which can easily be evaluated in terms of the quadrature nodes and weights.

2.4. The block case $\mathbf{u} \neq \mathbf{v}$

The block Lanczos iteration [11] produces a block tridiagonal Jacobi matrix J_K of order $2K$, which yields a block Gaussian quadrature rule that can be used for the case $\mathbf{u} \neq \mathbf{v}$. We have

$$J_K = \begin{bmatrix} M_1 & B_1^H & & & \\ B_1 & M_2 & B_2^H & & \\ & \ddots & \ddots & \ddots & \\ & & B_{K-2} & M_{K-1} & B_{K-1}^H \\ & & & B_{K-1} & M_K \end{bmatrix} \tag{12}$$

where, for $j = 1, 2, \ldots, K$,

$$R_{j-1} = X_j B_{j-1}, \quad M_j = X_j^H A X_j, \quad R_j = A X_j - X_j M_j - X_{j-1} B_{j-1}^H \tag{13}$$

where X_j is an $N \times 2$ matrix, $X_1^H X_1 = I$, B_j is 2×2 upper triangular and M_j is 2×2 symmetric [12]. The matrices X_j and B_{j-1} are obtained by performing a QR factorization of R_{j-1}. The initial value is $R_0 = \begin{bmatrix} \mathbf{u} & \mathbf{v} \end{bmatrix}$. Once J_K is obtained, a block Gaussian quadrature approximation of (7) is given by

$$\mathbf{u}^H f(A)\mathbf{v} = \mathbf{e}_1 B_0^H E_{12}^H f(J_K) E_{12} B_0 \mathbf{e}_2, \quad E_{12} = \begin{bmatrix} \mathbf{e}_1 & \mathbf{e}_2 \end{bmatrix}. \tag{14}$$

Please cite this article in press as: S. Sheikholeslami, J.V. Lambers, Modeling of first-order photobleaching kinetics using Krylov subspace spectral methods, Computers and Mathematics with Applications (2017), https://doi.org/10.1016/j.camwa.2017.10.019.

2.5. Block Arnoldi, $\mathbf{u} \neq \mathbf{v}$ case

The spatial differential operator for the system that we are solving is not self-adjoint, and therefore that would be discretized by an unsymmetric matrix. In the case of unsymmetric A, since the orthogonal tridiagonalization does not exist, we could instead obtain a block Hessenberg matrix H_K in place of the tridiagonal or block tridiagonal Jacobi matrix J_K. The block Hessenberg matrix H_K of order $2K$ for the block case $\mathbf{u} \neq \mathbf{v}$ can be written

$$H_K = \begin{bmatrix} H_{11} & H_{12} & H_{13} & \cdots & H_{1,K} \\ H_{21} & H_{22} & H_{23} & & \vdots \\ \vdots & \ddots & \ddots & \ddots & \vdots \\ 0 & 0 & H_{K-1,K-2} & H_{K-1,K-1} & H_{K-1,K} \\ 0 & 0 & 0 & H_{K,K-1} & H_{K,K} \end{bmatrix} \tag{15}$$

and for $j = 1, 2, \ldots, K$ and $i = 1, 2, \ldots, j$ we have

$$R_{j-1} = X_j H_{j,j-1}, \quad H_{ij} = X_i^H A X_j, \quad R_j = R_j - X_i H_{ij} \tag{16}$$

where $X_1^H X_1 = I$ [10] and R_0 is defined as before. As in the block Lanczos case, the eigenvalues and eigenvectors of H_K are used to construct a quadrature rule for the underlying Riemann–Stieltjes integral, which has the form (14) with H_K instead of J_K. Such quadrature rules are justified in [10] and the references therein.

The main reason for using block Arnoldi [13,14] is the loss of orthogonality of the Lanczos vectors in iterations which makes the unsymmetric Lanczos method unstable. In other words, iterations terminate while there is no invariant subspace information for A. Another problem with the unsymmetric Lanczos method is lack of convergence of eigenvalues and also serious breakdown [15].

For each time step and each frequency ω, the block KSS method proceeds by defining $R_0 = [\mathbf{u} \;\; \mathbf{v}] = \left[\frac{1}{\sqrt{2\pi}} e^{i\omega \mathbf{x}_N} \quad u(\mathbf{x}_N, t_n)\right]$ as the initial block for the block Arnoldi algorithm [15] described above, where $\mathbf{x}_N$ is a vector of equally spaced grid points. We compute the QR factorization $R_{j-1} = X_j H_{j,j-1}$. Then, block Arnoldi [13,14] is applied to produce the Hessenberg matrix H_K, which in turn yields the nodes and weights for the Gaussian quadrature rule needed to approximate each Fourier coefficient of the solution at time t_{n+1}. The details of these steps are discussed in the next two sections.

The temporal order of accuracy which has been reported for KSS methods applied to the heat equation [7], the wave equation [9], the Schrödinger equation [16], and Maxwell's equations [12] are $O(\Delta t^{(2K-1)d})$, where d is the highest order of a time derivative in the PDE. For the case $K = 1$, unconditional stability was proved for the parabolic [7] and hyperbolic [9] PDEs in 1-D, even though KSS methods are explicit. We will investigate the stability and convergence of the single-block node KSS method, as applied to Eq. (2), in future work.

3. Application of a first-order KSS method

In this section, we present the details of applying a first-order ($K = 1$) KSS method to (2). We seek a solution that is a linear combination of chosen basis functions, in which each coefficient in the linear combination is an expression of the form (7) that can be approximated using the approach outlined in Section 2. We begin with the construction of appropriate basis functions.

3.1. Construction of basis functions

For convenience, we use the spatial domain $E = [0, 2\pi]^2$, and impose periodic boundary conditions, as the initial data consists of constant functions and the evolution of the solution takes place in the interior of the domain. Homogeneous Dirichlet or Neumann boundary conditions can be handled in a similar manner [10]; we will discuss this in detail in Section 6.3. With this domain and boundary conditions, we use as our basis functions the eigenfunctions of a constant-coefficient problem obtained by averaging the variable coefficient $k_b I_{r_n}$, as described in [12].

Let $\omega = (\omega_1, \omega_2) \in \mathbb{Z}^2$. We denote points in E by $\mathbf{x} = (x, y)$. We define

$$L = \begin{bmatrix} -k_b I_{r_n}(\mathbf{x}) - k_{\text{on}} + D_1 \Delta & k_{\text{off}} \\ k_{\text{on}} & -k_b I_{r_n}(\mathbf{x}) - k_{\text{off}} + D_2 \Delta \end{bmatrix}, \quad \mathbf{v}(t) = \begin{bmatrix} u(\mathbf{x}, t) \\ b(\mathbf{x}, t) \end{bmatrix}, \tag{17}$$

then (2) takes the form $\mathbf{v}_t = L\mathbf{v}$. We now seek to solve a constant-coefficient approximation of this system of PDEs. To that end, the average of $I_{r_n}(\mathbf{x})$ over a rectangular domain E is given by

$$\bar{I}_{r_n} = \frac{1}{A(E)} \int\int_E I_{r_n}(x, y)\, dx\, dy = \frac{1}{A(E)} \int\int_{(x-x_c)^2+(y-y_c)^2 < r_n^2} \frac{I_0}{\pi r_n^2}\, dx\, dy = \frac{I_0}{A(E)}.$$

We then compute the 2×2 matrix

$$\bar{L}(\omega) = \begin{bmatrix} \langle e^{i\omega\cdot\mathbf{x}}, \bar{L}_{11} e^{i\omega\cdot\mathbf{x}} \rangle & \langle e^{i\omega\cdot\mathbf{x}}, \bar{L}_{12} e^{i\omega\cdot\mathbf{x}} \rangle \\ \langle e^{i\omega\cdot\mathbf{x}}, \bar{L}_{21} e^{i\omega\cdot\mathbf{x}} \rangle & \langle e^{i\omega\cdot\mathbf{x}}, \bar{L}_{22} e^{i\omega\cdot\mathbf{x}} \rangle \end{bmatrix},$$

Please cite this article in press as: S. Sheikholeslami, J.V. Lambers, Modeling of first-order photobleaching kinetics using Krylov subspace spectral methods, Computers and Mathematics with Applications (2017), https://doi.org/10.1016/j.camwa.2017.10.019.

where $\langle\cdot,\cdot\rangle$ is the standard L^2 inner product on E and, for $i, j = 1, 2$, $\bar{L}_{ij}$ is obtained from the entry L_{ij} of L by replacing I_{r_n} by $\bar{I}_{r_n}$. Then, the eigenvalues of $\bar{L}(\omega)$ are

$$\begin{aligned}\lambda_1 &= -\frac{k_b I_0}{A(E)} - \frac{1}{2}\|\omega\|^2(D_1+D_2) - \frac{1}{2}(k_{\text{on}}+k_{\text{off}}) + \\ &\quad \frac{1}{2}\left[\|\omega\|^4(D_1-D_2)^2 + \|\omega\|^2(2(D_1+D_2)(k_{\text{on}}+k_{\text{off}}) - \right. \\ &\quad \left. 4(D_1k_{\text{off}}+D_2k_{\text{on}})) + (k_{\text{on}}+k_{\text{off}})^2\right]^{1/2} \\ \lambda_2 &= -\frac{k_b I_0}{A(E)} - \frac{1}{2}\|\omega\|^2(D_1+D_2) - \frac{1}{2}(k_{\text{on}}+k_{\text{off}}) - \\ &\quad \frac{1}{2}\left[\|\omega\|^4(D_1-D_2)^2 + \|\omega\|^2(2(D_1+D_2)(k_{\text{on}}+k_{\text{off}}) - \right. \\ &\quad \left. 4(D_1k_{\text{off}}+D_2k_{\text{on}})) + (k_{\text{on}}+k_{\text{off}})^2\right]^{1/2}.\end{aligned}$$

If we write

$$\begin{bmatrix} u_{11} \\ u_{21} \end{bmatrix} = \begin{bmatrix} k_{\text{off}} \\ \dfrac{k_b I_0}{A(E)} + D_1\|\omega\|^2 + k_{\text{on}} + \lambda_1 \end{bmatrix} \tag{18}$$

then one eigenvector of $\bar{L}(\omega)$ is

$$\begin{bmatrix} u_{11} \\ u_{21} \end{bmatrix} = \begin{bmatrix} k_{\text{off}} \\ c_1 \end{bmatrix}$$

where

$$\begin{aligned}c_1 &= \frac{1}{2}\|\omega\|^2(D_1-D_2) + \frac{1}{2}(k_{\text{on}}-k_{\text{off}}) + \\ &\quad \frac{1}{2}\left[\|\omega\|^4(D_1-D_2)^2 + \|\omega\|^2(2(D_1+D_2)(k_{\text{on}}+k_{\text{off}}) - \right. \\ &\quad \left. 4(D_1k_{\text{off}}+D_2k_{\text{on}})) + (k_{\text{on}}+k_{\text{off}})^2\right]^{1/2}.\end{aligned}$$

If the eigenvalues λ_1 and λ_2 are distinct, then the eigenvector corresponding to λ_2 is given by

$$\begin{bmatrix} u_{12} \\ u_{22} \end{bmatrix} = \begin{bmatrix} k_{\text{off}} \\ c_2 \end{bmatrix}$$

where

$$\begin{aligned}c_2 &= \frac{1}{2}\|\omega\|^2(D_1-D_2) + \frac{1}{2}(k_{\text{on}}-k_{\text{off}}) - \\ &\quad \frac{1}{2}\left[\|\omega\|^4(D_1-D_2)^2 + \|\omega\|^2(2(D_1+D_2)(k_{\text{on}}+k_{\text{off}}) - \right. \\ &\quad \left. 4(D_1k_{\text{off}}+D_2k_{\text{on}})) + (k_{\text{on}}+k_{\text{off}})^2\right]^{1/2}.\end{aligned}$$

Let U be the 2×2 matrix with entries $u_{ij}, j = 1, 2$. By computing $V = U^{-T}$, we obtain the left eigenvectors of $\bar{L}(\omega)$:

$$\begin{aligned}U^{-1}(\omega) = V^T(\omega) &= \frac{1}{k_{\text{off}}(c_2-c_1)}\begin{bmatrix} c_2 & -c_1 \\ -k_{\text{off}} & k_{\text{off}} \end{bmatrix} \\ &= \frac{-1}{(D_1-D_2)(\omega_1^2+\omega_2^2)+(k_{\text{on}}-k_{\text{off}})}\begin{bmatrix} \dfrac{u_{22}}{k_{\text{off}}} & \dfrac{-u_{21}}{k_{\text{off}}} \\ -1 & 1 \end{bmatrix}.\end{aligned}$$

If we write

$$U(\omega) = \begin{bmatrix}\mathbf{u}_1(\omega)\ \mathbf{u}_2(\omega)\end{bmatrix}$$

and similar for $V(\omega)$, then the right and left eigenfunctions, respectively, of the frozen-coefficient operator $\bar{L}$ are, for $j = 1, 2$,

$$\begin{aligned}\mathbf{u}_{j,\omega}(\mathbf{x}) &= \mathbf{u}_j(\omega)\otimes e^{i(\omega\cdot\mathbf{x})} = \begin{bmatrix} u_{1j}e^{i(\omega\cdot\mathbf{x})} \\ u_{2j}e^{i(\omega\cdot\mathbf{x})} \end{bmatrix}, \\ \mathbf{v}_{j,\omega}(\mathbf{x}) &= \mathbf{v}_j(\omega)\otimes e^{i(\omega\cdot\mathbf{x})} = \begin{bmatrix} v_{1j}e^{i(\omega\cdot\mathbf{x})} \\ v_{2j}e^{i(\omega\cdot\mathbf{x})} \end{bmatrix}.\end{aligned}$$

Please cite this article in press as: S. Sheikholeslami, J.V. Lambers, Modeling of first-order photobleaching kinetics using Krylov subspace spectral methods, Computers and Mathematics with Applications (2017), https://doi.org/10.1016/j.camwa.2017.10.019.

If the eigenvalues λ_1 and λ_2 are equal, we use Schur vectors instead of eigenvectors, which entails setting

$$\begin{bmatrix} u_{12} \\ u_{22} \end{bmatrix} = \begin{bmatrix} -c_1 \\ k_{\text{off}} \end{bmatrix}$$

and computing $V(\omega) = U(\omega)/(k_{\text{off}}^2 + c_1^2)$.

Once we have obtained our basis functions for each $\omega \in \Omega \subset \mathbb{Z}^2$, where Ω is a chosen subset of frequency space determined by spatial discretization, we then seek a solution of (2) of the form

$$\begin{bmatrix} u(\mathbf{x}, t_{n+1}) \\ b(\mathbf{x}, t_{n+1}) \end{bmatrix} = \sum_{\omega \in \Omega} \sum_{j=1}^{2} \mathbf{u}_{j,\omega}(\mathbf{x}) \left\langle \mathbf{v}_{j,\omega}, e^{Lt} \begin{bmatrix} u(\mathbf{x}, t_n) \\ b(\mathbf{x}, t_n) \end{bmatrix} \right\rangle$$

where $\Delta t = t_{n+1} - t_n$ is a chosen time step. We can then approximate each inner product in the above linear combination by treating it as a Riemann–Stieltjes integral, as described in Section 2.

3.2. Block Arnoldi, $\omega \neq 0$

Now that our basis functions have been chosen, we will approximate each coefficient of the form

$$\left\langle \mathbf{v}_{j,\vec{\omega}}, \begin{bmatrix} u(\mathbf{x}, t_{n+1}) \\ b(\mathbf{x}, t_{n+1}) \end{bmatrix} \right\rangle = \left\langle \mathbf{v}_{j,\vec{\omega}}, e^{L\Delta t} \begin{bmatrix} u(\mathbf{x}, t_n) \\ b(\mathbf{x}, t_n) \end{bmatrix} \right\rangle, \quad j = 1, 2, \tag{19}$$

using a two-node block Gaussian quadrature rule. We begin with spatial discretization, using a uniform grid with spacing $\Delta x = \Delta y = 2\pi/N$, where for convenience we assume N is even. We denote by $\mathbf{x}_N$ a $N^2 \times 2$ matrix, the columns of which contain the x- and y-coordinates, respectively, of the grid points (x_i, y_j), $i, j = 0, 1, \ldots, N-1$, with $x_i = i\Delta x$ and $y_j = j\Delta y$. As before, we also denote by $\omega = (\omega_1, \omega_2)$ a pair of wave numbers, where $-N/2 + 1 \leq \omega_i \leq N/2$ for $i = 1, 2$. It follows that spatial error is introduced due to the truncation of the Fourier series of $u(\mathbf{x}, t)$ and $b(\mathbf{x}, t)$.

To approximate each coefficient (19), we perform a single iteration of block Arnoldi, with $N^2 \times 2$ initial blocks

$$R_0 = \begin{bmatrix} v_{11}(\omega)e^{i\omega\cdot\mathbf{x}_N} & u(\mathbf{x}_N, t_n) \\ v_{21}(\omega)e^{i\omega\cdot\mathbf{x}_N} & b(\mathbf{x}_N, t_n) \end{bmatrix}$$
$$\tilde{R}_0 = \begin{bmatrix} v_{12}(\omega)e^{i\omega\cdot\mathbf{x}_N} & u(\mathbf{x}_N, t_n) \\ v_{22}(\omega)e^{i\omega\cdot\mathbf{x}_N} & b(\mathbf{x}_N, t_n) \end{bmatrix}.$$

Before proceeding, we introduce the following notation for conciseness. First, we suppress the explicit dependence on $\mathbf{x}_N$ and t_n in the current solution:

$$u = u(\mathbf{x}_N, t_n), \quad b = b(\mathbf{x}_N, t_n).$$

Next, we use a similar shorthand for the discrete Fourier transforms, which implicitly depend on ω:

$$\hat{u} = (e^{i\omega\cdot\mathbf{x}_N})^H u, \quad \hat{b} = (e^{i\omega\cdot\mathbf{x}_N})^H b.$$

Throughout, we use $\|\cdot\|$ to refer to vector ℓ_2-norms.

Then, as the first step in block Arnoldi, we perform a QR factorization of R_0 and $\tilde{R}_0$, which yields

$$R_0 = X_1 B_0, \quad \tilde{R}_0 = \tilde{X}_1 \tilde{B}_0.$$

By defining

$$\begin{aligned} f &= uN^2\|\mathbf{v}_1(\omega)\|^2 - (v_{11}^2(\omega)\hat{u} + v_{21}(\omega)v_{11}(\omega)\hat{b})e^{i\omega\cdot\mathbf{x}_N} \\ g &= bN^2\|\mathbf{v}_1(\omega)\|^2 - (v_{21}^2(\omega)\hat{b} + v_{21}(\omega)v_{11}(\omega)\hat{u})e^{i\omega\cdot\mathbf{x}_N} \\ h &= uN^2\|\mathbf{v}_2(\omega)\|^2 - (v_{12}^2(\omega)\hat{u} + v_{22}(\omega)v_{12}(\omega)\hat{b})e^{i\omega\cdot\mathbf{x}_N} \\ k &= bN^2\|\mathbf{v}_2(\omega)\|^2 - (v_{22}^2(\omega)\hat{b} + v_{22}(\omega)v_{12}(\omega)\hat{u})e^{i\omega\cdot\mathbf{x}_N} \end{aligned}$$

we obtain

$$X_1 = \begin{bmatrix} x_{11} & x_{12} \end{bmatrix} = \begin{bmatrix} \dfrac{\begin{bmatrix} v_{11}(\omega)e^{i\omega\cdot\mathbf{x}_N} \\ v_{21}(\omega)e^{i\omega\cdot\mathbf{x}_N} \end{bmatrix}}{N\|\mathbf{v}_1(\omega)\|} & \dfrac{\begin{bmatrix} f \\ g \end{bmatrix}}{\sqrt{\|f\|^2 + \|g\|^2}} \end{bmatrix}$$
$$\tilde{X}_1 = \begin{bmatrix} \tilde{x}_{11} & \tilde{x}_{12} \end{bmatrix} = \begin{bmatrix} \dfrac{\begin{bmatrix} v_{12}(\omega)e^{i\omega\cdot\mathbf{x}_N} \\ v_{22}(\omega)e^{i\omega\cdot\mathbf{x}_N} \end{bmatrix}}{N\|\mathbf{v}_2(\omega)\|} & \dfrac{\begin{bmatrix} h \\ k \end{bmatrix}}{\sqrt{\|h\|^2 + \|k\|^2}} \end{bmatrix}. \tag{20}$$

It should be noted that if the columns of R_0 or $\tilde{R}_0$ are not linearly independent, then we can simply use the approach described in Section 2.3 to approximate our bilinear form (19), which is in this case effectively a quadratic form.

Please cite this article in press as: S. Sheikholeslami, J.V. Lambers, Modeling of first-order photobleaching kinetics using Krylov subspace spectral methods, Computers and Mathematics with Applications (2017), https://doi.org/10.1016/j.camwa.2017.10.019.

Then, M_1 and $\tilde{M}_1$, which correspond to H_{11} from the block Arnoldi algorithm, can be calculated by

$$\begin{aligned} M_1 &= X_1^H L X_1 \\ &= \begin{bmatrix} M_{11} & M_{12} \\ M_{21} & M_{22} \end{bmatrix} \end{aligned} \tag{21}$$

$$\begin{aligned} \tilde{M}_1 &= \tilde{X}_1^H L \tilde{X}_1 \\ &= \begin{bmatrix} \tilde{M}_{11} & \tilde{M}_{12} \\ \tilde{M}_{21} & \tilde{M}_{22} \end{bmatrix}. \end{aligned} \tag{22}$$

Formulas for the entries of M_1 and $\tilde{M}_1$ are given in Appendix A.1 of Appendix.

After computing the eigenvalues $\lambda_{1,\omega}$, $\lambda_{2,\omega}$ of M_1, the coefficient of $\mathbf{u}_{1,\omega}$ in the solution at time t can be approximated by

$$[B_0^H e^{M_1 \Delta t} B_0]_{12} = \left\langle \mathbf{v}_1(\omega) \otimes e^{i\omega \cdot \mathbf{x}_N}, \rho_\omega(L_N) \begin{bmatrix} u \\ b \end{bmatrix} \right\rangle$$

where ρ_ω is a polynomial of degree 1 which interpolates $e^{\lambda \Delta t}$ at $\lambda_{1,\omega}$ and $\lambda_{2,\omega}$ and is given by

$$\rho_\omega(L_N) = \frac{e^{\lambda_{1,\omega}\Delta t}}{\lambda_{1,\omega} - \lambda_{2,\omega}}[L_N - \lambda_{2,\omega} I] + \frac{e^{\lambda_{2,\omega}\Delta t}}{\lambda_{2,\omega} - \lambda_{1,\omega}}[L_N - \lambda_{1,\omega} I] \tag{23}$$

if $\lambda_{1,\omega} \neq \lambda_{2,\omega}$, based on Lagrange interpolation, or

$$\rho_\omega(L_N) = e^{\lambda_{1,\omega}\Delta t} I + \Delta t e^{\lambda_{1,\omega}\Delta t}(L_N - \lambda_{1,\omega} I) \tag{24}$$

if $\lambda_{1,\omega} = \lambda_{2,\omega}$, based on Hermite interpolation. The coefficient of $\mathbf{u}_{2,\omega}$ can be approximated in a similar manner, using the eigenvalues $\tilde{\lambda}_{1,\omega}$, $\tilde{\lambda}_{2,\omega}$ of $\tilde{M}_1$.

The value of Δt can be chosen sufficiently small to ensure desired accuracy, and then this process can be repeated in subsequent time steps. By using the integrand $g(\lambda) = \lambda e^{\lambda \Delta t}$ in place of $f(\lambda) = e^{\lambda \Delta t}$, one can easily use the above M_1 and $\tilde{M}_1$ to compute an approximate time derivative, which can then be used to obtain a residual $\mathbf{v}_t - L\mathbf{v}$. This residual can serve as an estimate of local truncation error, for the purpose of adaptive time-stepping.

3.3. Block Arnoldi, $\omega_1 = \omega_2 = 0$

We now use block Arnoldi for the case $\omega_1 = \omega_2 = 0$, for which we use the initial block

$$R_0 = \begin{bmatrix} \dfrac{-u_{22}}{k_{\text{off}}(k_{\text{on}} - k_{\text{off}})} & u(\mathbf{x}_N, t_n) \\ \dfrac{1}{k_{\text{on}} - k_{\text{off}}} & b(\mathbf{x}_N, t_n) \end{bmatrix}.$$

Then, after computing the QR factorization $R_0 = X_1 B_0$, we have

$$X_1 = \begin{bmatrix} \dfrac{1}{\sqrt{2}N} & \dfrac{u - \frac{\bar{u}+\bar{b}}{2}}{\sqrt{\|u\|^2 + \|b\|^2 - \frac{N^2(\bar{b}+\bar{u})^2}{2}}} \\ \dfrac{1}{\sqrt{2}N} & \dfrac{b - \frac{\bar{u}+\bar{b}}{2}}{\sqrt{\|u\|^2 + \|b\|^2 - \frac{N^2(\bar{b}+\bar{u})^2}{2}}} \end{bmatrix},$$

where we use $\bar{f}$ to denote the average of the components of a grid function f. Then, we compute $M_1 = X_1^H L X_1$. Formulas for the entries of M_1 are given in Appendix A.2. We then proceed as in the previous discussion to obtain the coefficient of $\mathbf{u}_{1,(0,0)}$ in the solution.

Similarly, for the coefficient of $\mathbf{u}_{2,(0,0)}$, our initial block is

$$\tilde{R}_0 = \begin{bmatrix} \dfrac{u_{21}}{k_{\text{off}}(k_{\text{on}} - k_{\text{off}})} & u(\mathbf{x}_N, t_n) \\ \dfrac{-1}{k_{\text{on}} - k_{\text{off}}} & b(\mathbf{x}_N, t_n) \end{bmatrix}.$$

Please cite this article in press as: S. Sheikholeslami, J.V. Lambers, Modeling of first-order photobleaching kinetics using Krylov subspace spectral methods, Computers and Mathematics with Applications (2017), https://doi.org/10.1016/j.camwa.2017.10.019.

Computing the QR factorization $\tilde{R}_0 = \tilde{X}_1\tilde{B}_0$ yields

$$\tilde{X}_1 = \begin{bmatrix} \dfrac{k_{\text{on}}}{N\sqrt{k_{\text{on}}^2+k_{\text{off}}^2}} & \dfrac{u(k_{\text{on}}^2+k_{\text{off}}^2)-k_{\text{on}}^2\bar{u}+k_{\text{on}}k_{\text{off}}\bar{b}}{\sqrt{d_{21}}} \\ \dfrac{-k_{\text{off}}}{N\sqrt{k_{\text{on}}^2+k_{\text{off}}^2}} & \dfrac{b(k_{\text{on}}^2+k_{\text{off}}^2)-k_{\text{off}}^2\bar{b}+k_{\text{on}}k_{\text{off}}\bar{u}}{\sqrt{d_{21}}} \end{bmatrix},$$

$$d_{21} = \|u\|^2+\|b\|^2-\frac{N^2\bar{u}^2k_{\text{on}}^2}{k_{\text{on}}^2+k_{\text{off}}^2}-\frac{N^2\bar{b}^2k_{\text{off}}^2}{k_{\text{on}}^2+k_{\text{off}}^2}+\frac{2N^2\bar{u}\bar{b}k_{\text{on}}k_{\text{off}}}{k_{\text{on}}^2+k_{\text{off}}^2}.$$

Then, we compute $\tilde{M}_1 = \tilde{X}_1^H L\tilde{X}_1$. Formulas for the entries of $\tilde{M}_1$ are given in Appendix A.2.

4. Approximate analytical solution

In this section, we specialize to initial data (3), (4) from pre-bleach steady states to obtain an approximate analytical solution for sufficiently small t. The terms in the entries of $V(\omega)$ that are of lower order in $\|\omega\|$ are neglected.

4.1. The $\omega \neq 0$ case

To facilitate analysis of high-frequency components, here we neglect lower-order terms in $\|\omega\|_2$. For the component of the solution in the directions of $\mathbf{u}_{1,\omega}$ and $\mathbf{u}_{2,\omega}$ with $\|\omega\| > 0$, the initial blocks are

$$R_0 = \begin{bmatrix} \dfrac{-1}{(D_1-D_2)\|\omega\|^2+(k_{\text{on}}-k_{\text{off}})} \begin{bmatrix} \dfrac{u_{22}e^{i\omega\cdot\mathbf{x}_N}}{k_{\text{off}}} \\ -e^{i\omega\cdot\mathbf{x}_N} \end{bmatrix} \begin{bmatrix} \dfrac{k_{\text{off}}c_i}{k_{\text{off}}+k_{\text{on}}} \\ \dfrac{k_{\text{on}}c_i}{k_{\text{off}}+k_{\text{on}}} \end{bmatrix} \end{bmatrix}.$$

$$\tilde{R}_0 = \begin{bmatrix} \dfrac{-1}{(D_1-D_2)\|\omega\|^2+(k_{\text{on}}-k_{\text{off}})} \begin{bmatrix} -\dfrac{u_{21}e^{i\omega\cdot\mathbf{x}_N}}{k_{\text{off}}} \\ e^{i\omega\cdot\mathbf{x}_N} \end{bmatrix} \begin{bmatrix} \dfrac{k_{\text{off}}c_i}{k_{\text{off}}+k_{\text{on}}} \\ \dfrac{k_{\text{on}}c_i}{k_{\text{off}}+k_{\text{on}}} \end{bmatrix} \end{bmatrix}.$$

Orthogonalization of these initial blocks yields

$$X_1 = \frac{1}{N\sqrt{u_{22}^2+k_{\text{off}}^2}}\begin{bmatrix} -u_{22}e^{i\omega\cdot\mathbf{x}_N} & k_{\text{off}} \\ k_{\text{off}}e^{i\omega\cdot\mathbf{x}_N} & u_{22} \end{bmatrix}, \quad \tilde{X}_1 = \frac{1}{N\sqrt{u_{21}^2+k_{\text{off}}^2}}\begin{bmatrix} u_{21}e^{i\omega\cdot\mathbf{x}_N} & k_{\text{off}} \\ -k_{\text{off}}e^{i\omega\cdot\mathbf{x}_N} & u_{21} \end{bmatrix}.$$

We then compute $M_1 = X_1^H LX_1$ and $\tilde{M}_1 = \tilde{X}_1^H L\tilde{X}_1$. Formulas for the entries of M_1 and $\tilde{M}_1$ are given in Appendix A.3.

As before, for $j = 1, 2$, let $\lambda_{j,\omega}$ and $\tilde{\lambda}_{j,\omega}$ denote the eigenvalues of M_1 and $\tilde{M}_1$, respectively. Formulas for these eigenvalues are also given in Appendix A.3. Then, the component of the solution in the direction of $\mathbf{u}_{1,\omega}$ is

$$[B_0^H e^{M_1 t}B_0]_{12} = \left\langle \mathbf{v}_1(\omega)\otimes e^{i\omega\cdot\mathbf{x}}, \rho_\omega(L)\begin{bmatrix} u(\mathbf{x},0) \\ b(\mathbf{x},0) \end{bmatrix} \right\rangle$$

where ρ_ω is a polynomial of degree 1 which interpolates $e^{\lambda t}$ at $\lambda_{1,\omega}$ and $\lambda_{2,\omega}$ given by (23) or (24), depending on whether $\lambda_{1,\omega}$ and $\lambda_{2,\omega}$ are distinct. The component in the direction of $\mathbf{u}_{2,\omega}$ can be computed similarly, by interpolating at $\tilde{\lambda}_{1,\omega}$ and $\tilde{\lambda}_{2,\omega}$. We conclude that the approximate analytical solution is

$$\begin{aligned} \begin{bmatrix} u(\mathbf{x},t) \\ b(\mathbf{x},t) \end{bmatrix} &= \sum_{\omega\in\mathbb{Z}^2} \mathbf{u}_{1,\omega}(\mathbf{x}) \left\langle \mathbf{v}_{1,\omega}, \rho_\omega(L)\begin{bmatrix} u(\mathbf{x},0) \\ b(\mathbf{x},0) \end{bmatrix} \right\rangle + \\ &\quad \sum_{\omega\in\mathbb{Z}^2} \mathbf{u}_{2,\omega}(\mathbf{x}) \left\langle \mathbf{v}_{2,\omega}, \tilde{\rho}_\omega(L)\begin{bmatrix} u(\mathbf{x},0) \\ b(\mathbf{x},0) \end{bmatrix} \right\rangle \\ &= \frac{-1}{(D_1-D_2)\|\omega\|^2+(k_{\text{on}}-k_{\text{off}})} \begin{bmatrix} u_{11}(\omega)e^{i\omega\cdot\mathbf{x}} \\ u_{21}(\omega)e^{i\omega\cdot\mathbf{x}} \end{bmatrix} \times \\ &\quad \begin{bmatrix} \dfrac{\overline{u_{22}}}{k_{\text{off}}}e^{-i\omega\cdot\mathbf{x}} & -e^{-i\omega\cdot\mathbf{x}} \end{bmatrix} \rho_\omega(L) \begin{bmatrix} \dfrac{k_{\text{off}}c_i}{k_{\text{off}}+k_{\text{on}}} \\ \dfrac{k_{\text{on}}c_i}{k_{\text{off}}+k_{\text{on}}} \end{bmatrix} + \end{aligned}$$

$$\frac{-1}{(D_1-D_2)\|\omega\|^2+(k_{\text{on}}-k_{\text{off}})}\begin{bmatrix}u_{12}(\omega)e^{i\omega\cdot\mathbf{x}}\\ u_{22}(\omega)e^{i\omega\cdot\mathbf{x}}\end{bmatrix}\times$$
$$\begin{bmatrix}\frac{-\overline{u_{21}}}{k_{\text{off}}}e^{-i\omega\cdot\mathbf{x}} & e^{-i\omega\cdot\mathbf{x}}\end{bmatrix}\tilde{\rho}_\omega(L)\begin{bmatrix}\frac{k_{\text{off}}c_i}{k_{\text{off}}+k_{\text{on}}}\\ \frac{k_{\text{on}}c_i}{k_{\text{off}}+k_{\text{on}}}\end{bmatrix}. \tag{25}$$

Here, we used exact basis functions which are valid for all frequencies, while in previous work [10] basis functions were approximated for the constant coefficient problem which were valid only at high frequencies.

4.2. The $\omega_1=\omega_2=0$ case

To complete the approximate analytical solution (25), we consider the special case $\omega_1=\omega_2=0$. Our initial block for the component in the direction of $\mathbf{u}_{1,(0,0)}$ is

$$R_0=\begin{bmatrix}-\frac{u_{22}}{k_{\text{off}}(k_{\text{on}}-k_{\text{off}})} & \frac{k_{\text{off}}c_i}{k_{\text{off}}+k_{\text{on}}}\\ \frac{1}{k_{\text{on}}-k_{\text{off}}} & \frac{k_{\text{on}}c_i}{k_{\text{off}}+k_{\text{on}}}\end{bmatrix}.$$

Substituting $u_{22}=-k_{\text{off}}$ in x_{11} and x_{12}, X_1 becomes

$$X_1=\begin{bmatrix}\frac{1}{\sqrt{2}N} & -\frac{1}{\sqrt{2}N}\\ \frac{1}{\sqrt{2}N} & \frac{1}{\sqrt{2}N}\end{bmatrix}$$

which yields

$$M_1=X_1^HLX_1=\begin{bmatrix}-k_b\overline{I_{r_n}} & 0\\ k_{\text{on}}-k_{\text{off}} & -k_b\overline{I_{r_n}}-(k_{\text{on}}+k_{\text{off}})\end{bmatrix}.$$

The eigenvalues of M_1 are

$$\lambda_{1,(0,0)}=-k_b\overline{I_{r_n}}$$
$$\lambda_{2,(0,0)}=-k_b\overline{I_{r_n}}-(k_{\text{on}}+k_{\text{off}}).$$

For the component of the solution in the direction of $\mathbf{u}_{2,(0,0)}$, we use the initial block

$$\tilde{R}_0=\begin{bmatrix}\frac{u_{21}}{k_{\text{off}}(k_{\text{on}}-k_{\text{off}})} & \frac{k_{\text{off}}c_i}{k_{\text{off}}+k_{\text{on}}}\\ \frac{-1}{k_{\text{on}}-k_{\text{off}}} & \frac{k_{\text{on}}c_i}{k_{\text{off}}+k_{\text{on}}}\end{bmatrix}$$

where the QR factorization variables obtained by substituting $u_{21}=k_{\text{on}}$ are

$$\tilde{X}_1=\begin{bmatrix}\tilde{x}_{11} & \tilde{x}_{12}\end{bmatrix}=\begin{bmatrix}\frac{k_{\text{on}}}{N\sqrt{(k_{\text{on}}^2+k_{\text{off}}^2)}} & \frac{k_{\text{off}}}{N\sqrt{(k_{\text{on}}^2+k_{\text{off}}^2)}}\\ \frac{-k_{\text{off}}}{N\sqrt{(k_{\text{on}}^2+k_{\text{off}}^2)}} & \frac{k_{\text{on}}}{N\sqrt{(k_{\text{on}}^2+k_{\text{off}}^2)}}\end{bmatrix}.$$

Then

$$\tilde{M}_1=\tilde{X}_1^HL\tilde{X}_1=\begin{bmatrix}-k_b\overline{I_{r_n}}-(k_{\text{on}}+k_{\text{off}}) & 0\\ k_{\text{on}}-k_{\text{off}} & -k_b\overline{I_{r_n}}\end{bmatrix}.$$

It follows that the eigenvalues of $\tilde{M}_1$ are

$$\tilde{\lambda}_{1,(0,0)}=-k_b\overline{I_{r_n}}-(k_{\text{on}}+k_{\text{off}})$$
$$\tilde{\lambda}_{2,(0,0)}=-k_b\overline{I_{r_n}}.$$

We then use the pairs of interpolation points $(\lambda_{1,(0,0)},\lambda_{2,(0,0)})$ and $(\tilde{\lambda}_{1,(0,0)},\tilde{\lambda}_{2,(0,0)})$, as in the $\omega\neq 0$ case, to compute the coefficients of the solution (25) in the directions of $\mathbf{u}_{1,(0,0)}$ and $\mathbf{u}_{2,(0,0)}$, respectively.

Please cite this article in press as: S. Sheikholeslami, J.V. Lambers, Modeling of first-order photobleaching kinetics using Krylov subspace spectral methods, Computers and Mathematics with Applications (2017), https://doi.org/10.1016/j.camwa.2017.10.019.

5. Implementation details

In this section we show how the KSS method for modeling first-order photobleaching kinetics can be implemented efficiently through vectorized polynomial interpolation. This approach can be used to produce an approximate analytical solution that can provide insight into qualitative behavior, using the formulas for the block Gaussian quadrature nodes given in Section 4, or a numerical solution through time-stepping, using the more general formulas for the nodes given in Section 3. In this section, we consider the latter case for concreteness. We use FFTs that produce frequency components corresponding to wave numbers in the range $-\frac{N}{2}+1 \leq \omega_i \leq \frac{N}{2}$, for $i = 1, 2$, where we continue to assume that N is even.

To carry out a time step from time $t_n = n\Delta t$ to time t_{n+1}, we first compute, for each $\omega = (\omega_1, \omega_2)$ with ω_i in the indicated range, the block Gaussian quadrature nodes $\lambda_{1,\omega}$, $\lambda_{2,\omega}$, $\tilde{\lambda}_{1,\omega}$, $\tilde{\lambda}_{2,\omega}$ from Section 3. Next, we compute the first-degree polynomial $\rho_\omega(\lambda)$ that interpolates $e^{\lambda\Delta t}$ at $\lambda_{1,\omega}$ and $\lambda_{2,\omega}$. The coefficients of $\rho_\omega(\lambda)$ in power form are given by

$$c_{1,\omega} = \begin{cases} \dfrac{f_{2,\omega} - f_{1,\omega}}{\lambda_{2,\omega} - \lambda_{1,\omega}} & \lambda_{1,\omega} \neq \lambda_{2,\omega} \\ \Delta t f_{1,\omega} & \lambda_{1,\omega} = \lambda_{2,\omega}, \end{cases}$$
$$c_{0,\omega} = f_{1,\omega} - c_{1,\omega}\lambda_{1,\omega},$$

where

$$f_{k,\omega} = e^{\lambda_{k,\omega}\Delta t}, \quad k = 1, 2.$$

The polynomial $\tilde{\rho}_\omega(\lambda)$ that interpolates $e^{\lambda\Delta t}$ at $\tilde{\lambda}_1$ and $\tilde{\lambda}_2$ is computed in a similar manner. We denote its coefficients by $\tilde{c}_{0,\omega}$ and $\tilde{c}_{1,\omega}$.

Next, we compute

$$\rho_\omega(L_N)\begin{bmatrix} u \\ b \end{bmatrix}_n = c_{0,\omega}\begin{bmatrix} u \\ b \end{bmatrix}_n + c_{1,\omega}\begin{bmatrix} p \\ q \end{bmatrix}_n, \tag{26}$$
$$\tilde{\rho}_\omega(L_N)\begin{bmatrix} u \\ b \end{bmatrix}_n = \tilde{c}_{0,\omega}\begin{bmatrix} u \\ b \end{bmatrix}_n + \tilde{c}_{1,\omega}\begin{bmatrix} p \\ q \end{bmatrix}_n, \tag{27}$$

where

$$\begin{bmatrix} u \\ b \end{bmatrix}_n = \begin{bmatrix} u(\mathbf{x}, t_n) \\ b(\mathbf{x}, t_n) \end{bmatrix}, \quad \begin{bmatrix} p \\ q \end{bmatrix}_n = L_N\begin{bmatrix} u \\ b \end{bmatrix}_n.$$

The application of the operator L through the matrix L_N can be performed using a finite difference discretization of the Laplacian, using the standard five-point stencil on our uniform grid, or using a 2-D FFT. The former approach is more efficient, but the latter yields spectral accuracy in space, rather than second-order accuracy. Regardless, the main error is the first-order temporal error.

Finally, the Fourier coefficients of the solution at time t_{n+1} are computed as follows:

$$\begin{aligned} \begin{bmatrix} \hat{u}(\omega, t_{n+1}) \\ \hat{b}(\omega, t_{n+1}) \end{bmatrix} &= \begin{bmatrix} u_{11}(\omega) \\ u_{21}(\omega) \end{bmatrix}\left\langle \mathbf{v}_{1,\omega}, \rho_\omega(L_N)\begin{bmatrix} u \\ b \end{bmatrix}_n \right\rangle + \begin{bmatrix} u_{12}(\omega) \\ u_{22}(\omega) \end{bmatrix}\left\langle \mathbf{v}_{2,\omega}, \tilde{\rho}_\omega(L_N)\begin{bmatrix} u \\ b \end{bmatrix}_n \right\rangle \\ &= \begin{bmatrix} u_{11}(\omega) \\ u_{21}(\omega) \end{bmatrix}[c_{0,\omega}(\overline{v_{11}}(\omega)\hat{u}(\omega) + \overline{v_{21}}(\omega)\hat{b}(\omega)) + c_{1,\omega}(\overline{v_{11}}(\omega)\hat{p}(\omega) + \overline{v_{21}}(\omega)\hat{q}(\omega))] + \\ &\quad \begin{bmatrix} u_{12}(\omega) \\ u_{22}(\omega) \end{bmatrix}[\tilde{c}_{0,\omega}(\overline{v_{12}}(\omega)\hat{u}(\omega) + \overline{v_{22}}(\omega)\hat{b}(\omega)) + \tilde{c}_{1,\omega}(\overline{v_{12}}(\omega)\hat{p}(\omega) + \overline{v_{22}}(\omega)\hat{q}(\omega))]. \end{aligned}$$

To compute $\hat{u}$ and $\hat{b}$, matrices of 2-D Fourier coefficients are multiplied component-wise. An inverse FFT yields the solution at time t_{n+1}. If we are only taking a single time step, the process described in this section is still used, but with the formulas for the nodes given in Section 4.

The resulting algorithm requires $O(N^2 \log N)$ floating-point operations per time step, where N is the number of grid points per dimension. While other methods that use a finite difference discretization require only $O(N^2)$ floating-point operations per time step, it will be seen in Section 6.2 that an accurate solution can still be obtained via KSS with much greater efficiency.

6. Numerical results

We now use numerical experiments to validate the formulas of the previous sections and examine the performance, in terms of accuracy, efficiency, and scalability, of a first-order KSS method applied to (2).

Please cite this article in press as: S. Sheikholeslami, J.V. Lambers, Modeling of first-order photobleaching kinetics using Krylov subspace spectral methods, Computers and Mathematics with Applications (2017), https://doi.org/10.1016/j.camwa.2017.10.019.

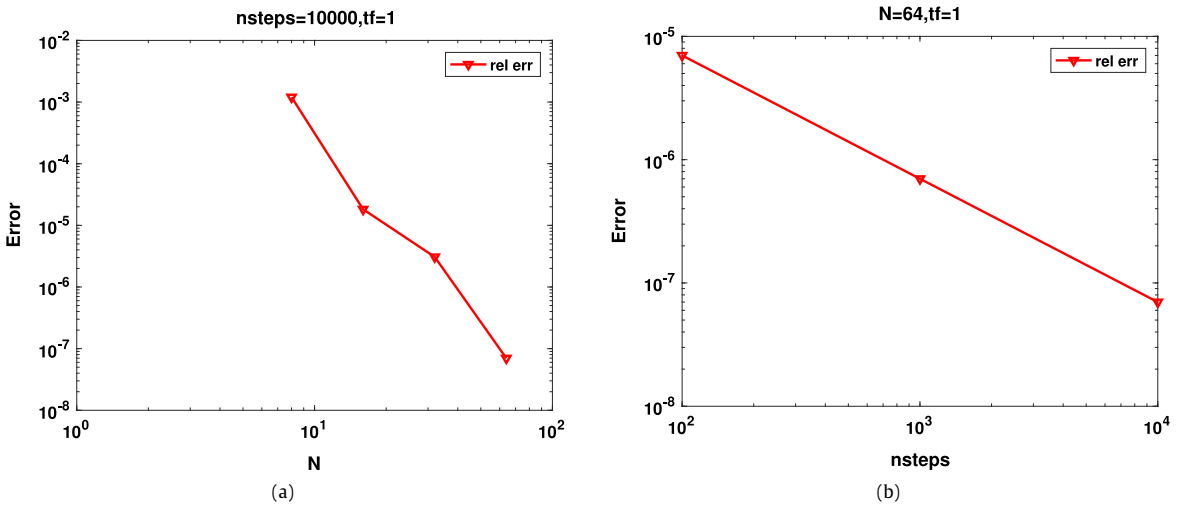

(a) (b)

Fig. 1. a: Relative error versus grid points (N). b: Relative error versus time steps. Parameters are $k_{\text{on}} = 10^{-0.5}$ s^{-1}, $k_{\text{off}} = 10^{-1}$ s^{-1}, $D_1 = 30$ μm^2/s, $D_2 = 10^{-4}$ μm^2/s and $\omega_{r_n} = 0.5$ μm.

Table 1
Execution time and relative error for different grid point for *nsteps* = 10,000 with parameters $k_{\text{on}} = 10^{-0.5}$ s^{-1}, $k_{\text{off}} = 10^{-1}$ s^{-1}, $D_1 = 30$ μm^2/s, $D_2 = 10^{-4}$ μm^2/s and $\omega_{r_n} = 0.5$ μm.

	$N = 8$	$N = 16$	$N = 32$	$N = 64$
Execution time (s)	4.4901	7.9654	19.7626	75.9164
Relative error	0.0012	1.8657e−05	3.6038e−06	6.9968e−08

Table 2
Execution time, and relative error for different grid point for $N = 64$ with parameters $k_{\text{on}} = 10^{-0.5}$ s^{-1}, $k_{\text{off}} = 10^{-1}$ s^{-1}, $D_1 = 30$ μm^2/s, $D_2 = 10^{-4}$ μm^2/s and $\omega_{r_n} = 0.5$ μm.

	Time steps = 100	Time steps = 1000	Time steps = 10 000
Execution time (s)	0.79309	6.8334	75.9164
Relative error	7.0045e−06	6.9974e−07	6.9968e−08

6.1. Validation of time-stepping scheme

First, we use the formulas of Section 3 to implement a time-stepping method, as described in Section 5. We present the relative error versus number of grid points per dimension (N) and number of time steps (*nsteps*). Errors are computed by comparing the solution at the final time (denoted by t_f) to that obtained by computing $e^{L_N t_f}$ times the initial data, using the MATLAB function `expm`. In all cases, we use the parameter values $k_b = 1$ and $c_i = 1$. The center (x_c, y_c) of the laser profile is set to be (π, π).

For our first test case, reaction-dominant parameters that are defined in Chapter 1 are set to be $k_{\text{on}} = 10^{-0.5}$ s^{-1}, $k_{\text{off}} = 10^{-1}$ s^{-1}, $D_1 = 30$ μm^2/s, $D_2 = 10^{-4}$ μm^2/s and $\omega_{r_n} = 0.5$ μm for Fig. 1. These values are taken from [4,17,18]. Fig. 1a shows relative error versus grid points (N) for *nsteps* = 10,000 (number of time steps) and final time $t_f = 1$. It shows a rapidly decreasing trend for relative error with increasing N. This is due to each solution being compared to an approximate solution computing using the matrix exponential on a finer grid. Fig. 1b shows relative error versus time steps for $N = 64$ and final time $t_f = 1$, corresponding to a time step $\Delta t = 1/nsteps$. It shows first-order accuracy in time, as expected. Table 1 shows the execution time and relative error for different grid sizes for *nsteps* = 10,000 with parameters $k_{\text{on}} = 10^{-0.5}$ s^{-1}, $k_{\text{off}} = 10^{-1}$ s^{-1}, $D_1 = 30$ μm^2/s, $D_2 = 10^{-4}$ μm^2/s and $\omega_{r_n} = 0.5$ μm. Table 2 shows the execution time and relative error for different time step sizes, with $N = 64$, for the same parameters.

For the second case, pure diffusion parameter values are set to be $k_{\text{on}} = 10^{-2}$ s^{-1}, $k_{\text{off}} = 10$ s^{-1}, $D_1 = 30$ μm^2/s, $D_2 = 10^{-4}$ μm^2/s and $\omega_{r_n} = 0.5$ μm for Fig. 2. Fig. 2a shows relative error versus grid points per dimension (N) for *nsteps* = 10,000 and $t_f = 1$. It shows a rapidly decreasing trend for relative error with increasing N. Fig. 2b shows relative error versus number of time steps for $N = 64$ and $t_f = 1$. As before, first-order accuracy in time is obtained. Table 3 shows the execution time and relative error for different grid point for *nsteps* = 10,000 with parameters $k_{\text{on}} = 10^{-2}$ s^{-1}, $k_{\text{off}} = 10$ s^{-1}, $D_1 = 30$ μm^2/s, $D_2 = 10^{-4}$ μm^2/s, $\omega_{r_n} = 0.5$ μm. Table 4 shows the execution time and relative error for different time steps, with $N = 64$, for the same parameters.

Please cite this article in press as: S. Sheikholeslami, J.V. Lambers, Modeling of first-order photobleaching kinetics using Krylov subspace spectral methods, Computers and Mathematics with Applications (2017), https://doi.org/10.1016/j.camwa.2017.10.019.

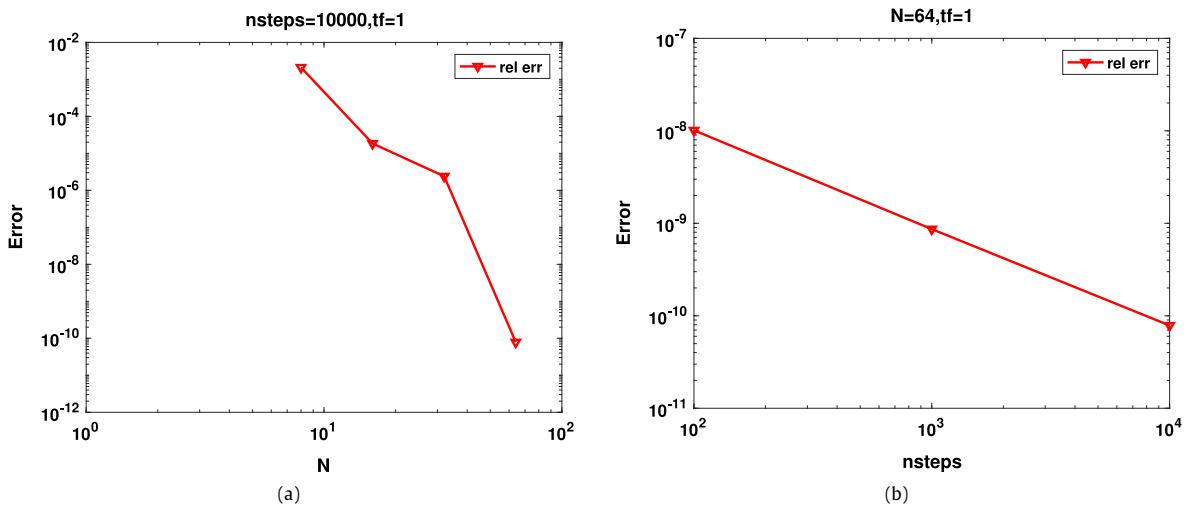

(a) (b)

Fig. 2. a: Relative error versus grid points (N). b: Relative error versus time steps. Parameters are $k_{on} = 10^{-2}$ s^{-1}, $k_{off} = 10$ s^{-1}, $D_1 = 30\ \mu$m^2/s, $D_2 = 10^{-4}$ μm^2/s and $\omega_{r_n} = 0.5\ \mu$m.

Table 3
Execution time and relative error for different grid point for *nsteps* = 10,000 with parameters $k_{on} = 10^{-2}$ s^{-1}, $k_{off} = 10$ s^{-1}, $D_1 = 30\ \mu$m^2/s, $D_2 = 10^{-4}$ μm^2/s and $\omega_{r_n} = 0.5\ \mu$m.

	$N = 8$	$N = 16$	$N = 32$	$N = 64$
Execution time (s)	4.6127	7.9169	19.9402	70.3547
Relative error	0.0021	1.8470e−05	2.4014e−06	7.8543e−11

Table 4
Execution time and relative error for different grid point for $N = 64$ with parameters $k_{on} = 10^{-2}$ s^{-1}, $k_{off} = 10$ s^{-1}, $D_1 = 30\ \mu$m^2/s, $D_2 = 10^{-4}$ μm^2/s and $\omega_{r_n} = 0.5\ \mu$m.

	Time steps = 100	Time steps = 1000	Time steps = 10 000
Execution time (s)	0.81812	6.9748	70.3547
Relative error	1.0130e−08	8.6496e−10	7.8543e−11

Table 5
Execution time and relative error for different grid point for *nsteps* = 10,000 with parameters $k_{on} = 10^{2}$ s^{-1}, $k_{off} = 10^{-1}$ s^{-1}, $D_1 = 30\ \mu$m^2/s, $D_2 = 10^{-1}$ μm^2/s and $\omega_{r_n} = 0.5\ \mu$m.

	$N = 8$	$N = 16$	$N = 32$	$N = 64$
Execution time (s)	4.5256	8.0008	20.7176	76.6904
Relative error	0.0100	9.6420e−04	1.7973e−04	3.0811e−08

Table 6
Execution time and relative error for different grid point for $N = 64$ with parameters $k_{on} = 10^{2}$ s^{-1}, $k_{off} = 10^{-1}$ s^{-1}, $D_1 = 30\ \mu$m^2/s, $D_2 = 10^{-1}$ μm^2/s and $\omega_{r_n} = 0.5\ \mu$m.

	Time steps = 100	Time steps = 1000	Time steps = 10 000
Execution time (s)	0.78111	7.6507	76.6904
Relative error	3.0821e−06	3.0810e−07	3.0811e−08

For the third case, full model parameter values are set to be $k_{on} = 10^{2}$ s^{-1}, $k_{off} = 10^{-1}$ s^{-1}, $D_1 = 30\ \mu$m^2/s, $D_2 = 10^{-1}$ μm^2/s and $\omega_{r_n} = 0.5\ \mu$m for Fig. 3. Here we consider a diffusion-dominated case. Fig. 3 shows relative error versus grid points per dimension (N) for *nsteps* = 10,000 and $t_f = 1$. As in the previous cases, it shows a decreasing trend for relative error by increasing N. Fig. 3b shows relative error versus time steps for $N = 64$ and $t_f = 1$. First-order accuracy in time is again observed. Table 5 shows the execution time and relative error for different grid sizes with *nsteps* = 10,000 and parameters $k_{on} = 10^{2}$ s^{-1}, $k_{off} = 10^{-1}$ s^{-1}, $D_1 = 30\ \mu$m^2/s, $D_2 = 10^{-1}$ μm^2/s and $\omega_{r_n} = 0.5\ \mu$m. Table 6 shows the execution time and relative error for different time step sizes with $N = 64$ for the same parameters.

It is particularly interesting to note that these test cases, the Courant–Friedrichs–Lewy (CFL) condition for forward Euler with $N = 64$ would require 10^5 time steps to ensure stability, but this KSS method, an explicit method, is able to not only ensure stability but also high accuracy even when greatly exceeding this CFL limit.

Please cite this article in press as: S. Sheikholeslami, J.V. Lambers, Modeling of first-order photobleaching kinetics using Krylov subspace spectral methods, Computers and Mathematics with Applications (2017), https://doi.org/10.1016/j.camwa.2017.10.019.

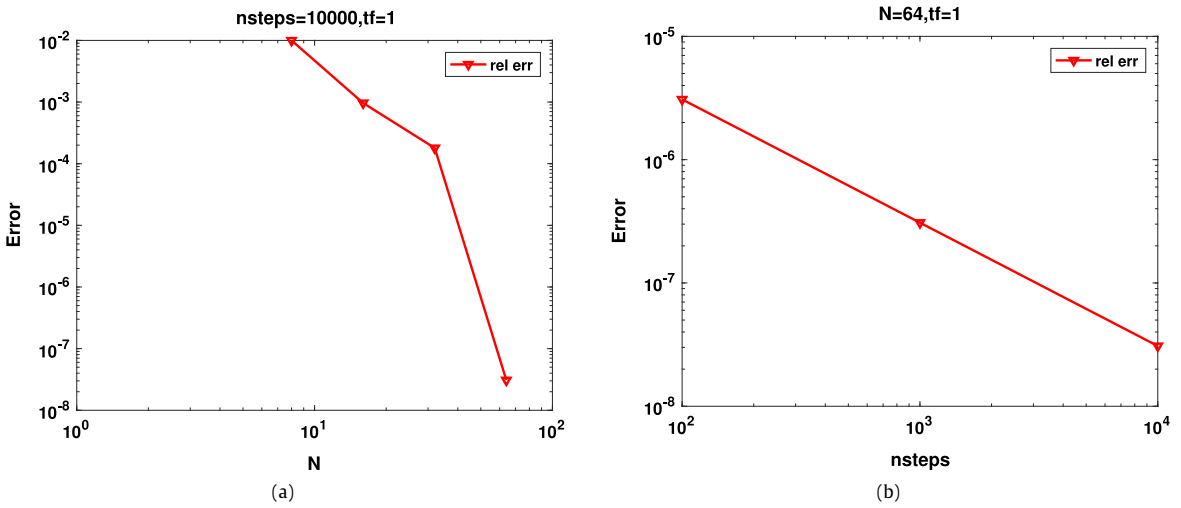

(a) (b)

Fig. 3. a: Relative error versus grid points (N). b: Relative error versus time steps. Parameters are $k_{on} = 10^2$ s^{-1}, $k_{off} = 10$ s^{-1}, $D_1 = 30$ μm^2/s, $D_2 = 10^{-1}$ μm^2/s and $\omega_{r_n} = 0.5$ μm.

Table 7
Execution time and relative error for the solution of (2) using a 1-node KSS method, Crank–Nicolson (CN), fourth-order Runge–Kutta (rk4), and forward Euler, for the reaction-dominant case from Table 1.

Periodic boundary conditions, reaction dominant case					
	Time steps	$N = 32$		$N = 64$	
		Execution time (s)	Rel error	Execution time (s)	Rel error
KSS	1	0.0018	7.7769e−04	0.0023	7.7768e−04
CN	1	0.0131	2.0654e−04	0.0611	2.0335e−04
rk4	10,000	1.5401	3.0146e−06	6.9910	4.5533e−13
Euler	100,000	2.3200	3.0241e−06	7.3987	1.4126e−08

6.2. Performance comparison

In this section we compare the performance of KSS with various other time-stepping methods: forward Euler, fourth-order Runge–Kutta, and Crank–Nicolson. For all methods, the standard 5-point finite difference stencil is used for the Laplacian. The results are shown in Table 7. For both KSS and Crank–Nicolson, only one time step is necessary to obtain a reasonably accurate solution, and we see that the accuracy of the two methods is comparable. However, KSS is significantly faster, and this advantage increases with the number of grid points N. Because forward Euler and fourth-order Runge–Kutta are explicit, a very small time step is required to obtain a viable solution, resulting in these methods being literally thousands of times slower than KSS.

For KSS, two optimizations were made. First, based on observations that the off-diagonal entries of M_1 and $\tilde{M}_1$ were, for most frequencies [19], negligibly small compared to the diagonal entries, only the diagonal entries were computed, and then used as the nodes. Second, the formulas in Section 5 were simplified to account for the fact that the components of the initial data are constant functions, which would mean that $\hat{u}$ and $\hat{b}$ would have only one nonzero component.

6.3. Changing boundary conditions

We now explain how we can solve (2) using homogeneous Neumann boundary conditions, rather than periodic boundary conditions. The following modifications are needed:

- Using discrete cosine transforms instead of the FFT
- Using frequency ranges $\omega_i = k/2$ for $i = 1, 2$ and $k = 0, 1, 2, \ldots, N-1$
- Using the appropriate finite difference discretization of the Laplacian, if applicable.

The formulas derived in Section 4 can still be used, for the appropriate values of ω, as the resulting quadrature nodes will have the necessary asymptotic behavior, as demonstrated in [10]. Table 8 shows the results of repeating the experiments of Section 6.2, but with Neumann boundary conditions. We see that all methods exhibit similar accuracy and efficiency.

Please cite this article in press as: S. Sheikholeslami, J.V. Lambers, Modeling of first-order photobleaching kinetics using Krylov subspace spectral methods, Computers and Mathematics with Applications (2017), https://doi.org/10.1016/j.camwa.2017.10.019.

Table 8
Execution time and relative error for the solution of (2) using a 1-node KSS method, Crank–Nicolson (CN), fourth-order Runge–Kutta (rk4), and forward Euler, for the reaction-dominant case from Table 1, except with homogeneous Neumann boundary conditions.

Neumann boundary condition, reaction dominant case					
	Time steps	$N = 32$		$N = 64$	
		Execution time (s)	Rel error	Execution time (s)	Rel error
KSS	1	0.0014	7.7774e−04	0.0049	7.7768e−04
CN	1	0.0127	2.0801e−04	0.0470	2.0346e−04
rk4	10,000	1.5437	1.1359e−05	6.7514	6.5951e−13
Euler	100,000	3.0507	1.1369e−05	7.4302	1.4126e−08

7. Conclusion

We applied a first-order KSS method to solve the first-order photobleaching kinetics partial differential equations with general initial conditions and the initial conditions that came from a pre-bleach steady state. It has been shown that by applying block Arnoldi iteration symbolically for each Fourier coefficient, an approximate analytical solution can be obtained that facilitates qualitative analysis of short-time behavior, which is relevant to the photobleaching stage. The numerical results indicate satisfactory accuracy of the method for all cases, which is promising for application to FRAP laboratory research. We present an approximate analytical solution to this model which makes qualitative analysis feasible for scientists in the field of cell biology.

Future work will consist of proving stability and convergence, consideration of more general laser profiles, and other generalizations of interest, including to three-dimensional problems as in [2]. In [12] KSS was applied to Maxwell's equations in 3-D; application to a 3-D version of (2) would be analogous. In fact, the approach described in this paper can be used without modification to the formulas herein, except with appropriately adjusted definitions of ω, L_N and I_{r_n}. Efficient application of higher-order KSS methods (that is, $K > 1$) will also be investigated. Also of interest are more general models in which the coefficients vary over time, as would be the case for modeling both photobleaching and recovery, for either a system of linear or nonlinear PDEs. For this case, a combination of KSS and EPI methods [20] introduced in [10] can be applied, in which KSS methods are used to approximate required matrix function-vector products.

Appendix

A.1. Block Arnoldi, $\omega \neq 0$

Here, we present formulas for the entries of M_1 and $\tilde{M}_1$ from Eqs. (21) and (22), respectively. We first define

$$\begin{aligned}
T_1 &= v_{11}^2(\omega)\hat{u} + v_{21}(\omega)v_{11}(\omega)\hat{b}\\
T_2 &= v_{21}^2(\omega)\hat{b} + v_{21}(\omega)v_{11}(\omega)\hat{u}\\
T_3 &= v_{11}^2(\omega)\overline{\hat{u}} + \overline{v_{21}(\omega)v_{11}(\omega)}\overline{\hat{b}}\\
T_4 &= v_{21}^2(\omega)\overline{\hat{b}} + \overline{v_{21}(\omega)v_{11}(\omega)}\overline{\hat{u}}\\
T_5 &= v_{12}^2(\omega)\hat{u} + v_{22}(\omega)v_{12}(\omega)\hat{b}\\
T_6 &= v_{22}^2(\omega)\hat{b} + v_{22}(\omega)v_{12}(\omega)\hat{u}\\
T_7 &= v_{12}^2(\omega)\overline{\hat{u}} + \overline{v_{22}(\omega)v_{12}(\omega)}\overline{\hat{b}}\\
T_8 &= v_{22}^2(\omega)\overline{\hat{b}} + \overline{v_{22}(\omega)v_{12}(\omega)}\overline{\hat{u}}.
\end{aligned}$$

Then, for M_1, we have

$$\begin{aligned}
M_{11} &= -k_b\overline{I_{r_n}} + \frac{n_1}{\|\mathbf{v}_1(\omega)\|^2}\\
M_{12} &= \frac{n_2}{d_1}\\
M_{21} &= \frac{n_3}{d_1}\\
M_{22} &= \frac{n_4}{d_2}
\end{aligned}$$

while for $\tilde{M}_1$, we have

$$\tilde{M}_{11} = -k_b\overline{I_{r_n}} + \frac{n_5}{\|\mathbf{v}_2(\omega)\|^2}$$

Please cite this article in press as: S. Sheikholeslami, J.V. Lambers, Modeling of first-order photobleaching kinetics using Krylov subspace spectral methods, Computers and Mathematics with Applications (2017), https://doi.org/10.1016/j.camwa.2017.10.019.

$$\tilde{M}_{12} = \frac{n_6}{d_3}$$
$$\tilde{M}_{21} = \frac{n_7}{d_3}$$
$$\tilde{M}_{22} = \frac{n_8}{d_4}$$

where

$$\begin{aligned}
n_1 &= k_{\text{off}}\overline{v_{11}(\omega)}v_{21}(\omega) + k_{\text{on}}\overline{v_{21}(\omega)}v_{11}(\omega) - (D_1 v_{11}^2(\omega) + D_2 v_{21}^2(\omega))\|\omega\|^2 - k_{\text{off}}v_{21}^2(\omega) - \\
&\quad k_{\text{on}}v_{11}^2(\omega) \\
n_2 &= -k_b\|\mathbf{v}_1(\omega)\|^2(\widehat{I_{r_n}u}\overline{v_{11}(\omega)} + \widehat{I_{r_n}b}\overline{v_{21}(\omega)}) + k_b\overline{I_{r_n}}[T_1\overline{v_{11}(\omega)} + T_2\overline{v_{21}(\omega)}] - \\
&\quad \|\omega\|^2\|\mathbf{v}_1(\omega)\|^2(D_1\overline{v_{11}(\omega)}\hat{u} + D_2\overline{v_{21}(\omega)}\hat{b}) + \|\omega\|^2[D_1\overline{v_{11}(\omega)}T_1 + D_2\overline{v_{21}(\omega)}T_2] + \\
&\quad \|\mathbf{v}_1(\omega)\|^2(\overline{v_{11}(\omega)}(k_{\text{off}}\hat{b} - k_{\text{on}}\hat{u}) + \overline{v_{21}(\omega)}(k_{\text{on}}\hat{u} - k_{\text{off}}\hat{b})) + \\
&\quad (\overline{v_{11}(\omega)} - \overline{v_{21}(\omega)})[k_{\text{on}}T_1 - k_{\text{off}}T_2] \\
n_3 &= -k_b\|\mathbf{v}_1(\omega)\|^2(\widehat{I_{r_n}u}v_{11}(\omega) + \widehat{I_{r_n}b}v_{21}(\omega)) + k_b\overline{I_{r_n}}[T_3 v_{11}(\omega) + T_4 v_{21}(\omega)] - \\
&\quad \|\omega\|^2\|\mathbf{v}_1(\omega)\|^2(D_1 v_{11}(\omega)\bar{\hat{u}} + D_2 v_{21}(\omega)\bar{\hat{b}}) + \|\omega\|^2[D_1 v_{11}(\omega)T_3 + D_2 v_{21}(\omega)T_4] + \\
&\quad \|\mathbf{v}_1(\omega)\|^2(v_{11}(\omega)(k_{\text{on}}\bar{\hat{b}} - k_{\text{on}}\bar{\hat{u}}) + v_{21}(\omega)(k_{\text{off}}\bar{\hat{u}} - k_{\text{off}}\bar{\hat{b}})) + \\
&\quad (v_{11}(\omega)k_{\text{on}} - v_{21}(\omega)k_{\text{off}})[T_3 - T_4]
\end{aligned}$$

$$\begin{aligned}
d_1 &= \sqrt{\|\mathbf{v}_1(\omega)\|^2} \times \\
&\quad N\sqrt{\|\mathbf{v}_1(\omega)\|^2(\|u^2\| + \|b^2\|) - \mathit{Real}(2\|\mathbf{v}_1(\omega)\|^2[\bar{\hat{u}}T_1 + \bar{\hat{b}}T_2]) + [(T_2)^2 + (T_1)^2]} \\
d_2 &= N^2\|\mathbf{v}_1(\omega)\|^2(\|u^2\| + \|b^2\|) - \mathit{Real}(2\|\mathbf{v}_1(\omega)\|^2[\bar{\hat{u}}T_1 + \bar{\hat{b}}T_2]) + [(T_2)^2 + (T_1)^2]
\end{aligned}$$

$$\begin{aligned}
n_4 &= [-k_{\text{off}}(T_2)^2 - k_{\text{on}}(T_1)^2] + k_{\text{on}}T_1T_4 + k_{\text{off}}T_3T_2 - N^4k_b\|\mathbf{v}_1(\omega)\|^4(\widehat{I_{r_n}u^2} + \widehat{I_{r_n}b^2}) + \\
&\quad k_b\|\mathbf{v}_1(\omega)\|^2[\widehat{I_{r_n}u}T_3 + \widehat{I_{r_n}b}T_4] - N^2\|\mathbf{v}_1(\omega)\|^4(D_1\|\nabla u\|^2 + D_2\|\nabla b\|^2) - \\
&\quad \|\mathbf{v}_1(\omega)\|^2T_1[-k_{\text{on}}\bar{\hat{b}} + D_1\|\omega\|^2\bar{\hat{u}} + k_{\text{on}}\bar{\hat{u}}] + \|\mathbf{v}_1(\omega)\|^2T_2[-k_{\text{off}}\bar{\hat{u}} + D_2\|\omega\|^2\bar{\hat{b}} + k_{\text{off}}\bar{\hat{b}}] - \\
&\quad k_b\overline{I_{r_n}}[(T_2)^2 + (T_1)^2] + (k_{\text{off}}\hat{b} - k_{\text{on}}\hat{u})\|\mathbf{v}_1(\omega)\|^2T_4 - \\
&\quad \|\omega\|^2[D_1(T_3)^2 + D_2(T_4)^2] + (k_{\text{on}}\hat{u} - k_{\text{off}}\hat{b})\|\mathbf{v}_1(\omega)\|^2T_3 + \\
&\quad N^2\|\mathbf{v}_1(\omega)\|^4[-k_{\text{on}}\|u\|^2 + N^2k_{\text{off}}\overline{ub} + N^2k_{\text{on}}\overline{bu} - k_{\text{off}}\|b\|^2] - \\
&\quad \|\omega\|^2\|\mathbf{v}_1(\omega)\|^2[D_1\hat{u}T_3 + D_2\hat{b}T_4] + k_b\|\mathbf{v}_1(\omega)\|^2[\widehat{I_{r_n}b}T_2 + \widehat{I_{r_n}u}T_1] \\
n_5 &= k_{\text{off}}\overline{v_{12}(\omega)}v_{22}(\omega) + k_{\text{on}}\overline{v_{22}(\omega)}v_{12}(\omega) - (D_1 v_{12}^2(\omega) + D_2 v_{22}^2(\omega))\|\omega\|^2 - k_{\text{off}}v_{22}^2(\omega) - \\
&\quad k_{\text{on}}v_{12}^2(\omega) \\
n_6 &= -k_b\|\mathbf{v}_2(\omega)\|^2(\widehat{I_{r_n}u}\overline{v_{12}(\omega)} + \widehat{I_{r_n}b}\overline{v_{22}(\omega)}) + k_b\overline{I_{r_n}}[T_5\overline{v_{12}(\omega)} + T_6\overline{v_{22}(\omega)}] - \\
&\quad \|\omega\|^2\|\mathbf{v}_2(\omega)\|^2(D_1\overline{v_{12}(\omega)}\hat{u} + D_2\overline{v_{22}(\omega)}\hat{b}) + \|\omega\|^2[D_1\overline{v_{12}(\omega)}T_5 + D_2\overline{v_{22}(\omega)}T_6] + \\
&\quad \|\mathbf{v}_2(\omega)\|^2(\overline{v_{12}(\omega)}(k_{\text{off}}\hat{b} - k_{\text{on}}\hat{u}) + \overline{v_{22}(\omega)}(k_{\text{on}}\hat{u} - k_{\text{off}}\hat{b})) + \\
&\quad (\overline{v_{12}(\omega)} - \overline{v_{22}(\omega)})[k_{\text{on}}T_5 - k_{\text{off}}T_6] \\
n_7 &= -k_b\|\mathbf{v}_2(\omega)\|^2\widehat{I_{r_n}u}v_{12}(\omega) + \widehat{I_{r_n}b}v_{22}(\omega) + k_b\overline{I_{r_n}}[T_7 v_{12}(\omega) + T_8 v_{22}(\omega)] - \\
&\quad \|\omega\|^2\|\mathbf{v}_2(\omega)\|^2(D_1 v_{12}(\omega)\bar{\hat{u}} + D_2 v_{22}(\omega)\bar{\hat{b}}) + \|\omega\|^2[D_1 v_{12}(\omega)T_7 + D_2 v_{22}(\omega)T_8] + \\
&\quad \|\mathbf{v}_2(\omega)\|^2(v_{12}(\omega)(k_{\text{on}}\bar{\hat{b}} - k_{\text{on}}\bar{\hat{u}}) + v_{22}(\omega)(k_{\text{off}}\bar{\hat{u}} - k_{\text{off}}\bar{\hat{b}})) + \\
&\quad (v_{12}(\omega)k_{\text{on}} - v_{22}(\omega)k_{\text{off}})[T_7 - T_8]
\end{aligned}$$

$$\begin{aligned}
d_3 &= \sqrt{\|\mathbf{v}_2(\omega)\|^2} \times \\
&\quad \sqrt{N^2\|\mathbf{v}_2(\omega)\|^2(\|u^2\| + \|b^2\|) - \mathit{Real}(2\|\mathbf{v}_2(\omega)\|^2[\bar{\hat{u}}T_5 + \bar{\hat{b}}T_6]) + [(T_6)^2 + (T_5)^2]} \\
d_4 &= N^2\|\mathbf{v}_2(\omega)\|^2(\|u^2\| + \|b^2\|) - \mathit{Real}(2\|\mathbf{v}_2(\omega)\|^2[\bar{\hat{u}}T_5 + \bar{\hat{b}}T_6]) + [(T_6)^2 + (T_5)^2]
\end{aligned}$$

Please cite this article in press as: S. Sheikholeslami, J.V. Lambers, Modeling of first-order photobleaching kinetics using Krylov subspace spectral methods, Computers and Mathematics with Applications (2017), https://doi.org/10.1016/j.camwa.2017.10.019.

$$
\begin{aligned}
n_8 = {} & [-k_{\text{off}}(T_6)^2 - k_{\text{on}}(T_5)^2] + k_{\text{on}}T_5T_8 + k_{\text{off}}T_7T_6 - N^4k_b\|\mathbf{v}_2(\omega)\|^4(\widehat{\overline{I_{r_n}u^2}} + \widehat{\overline{I_{r_n}b^2}}) + \\
& k_b\|\mathbf{v}_2(\omega)\|^2[\widehat{\overline{I_{r_n}}u}T_7 + \widehat{\overline{I_{r_n}}b}T_8] - N^2\|\mathbf{v}_2(\omega)\|^4(D_1\|\nabla u\|^2 + D_2\|\nabla b\|^2) - \\
& \|\mathbf{v}_2(\omega)\|^2T_5[-k_{\text{on}}\bar{\hat{b}} + D_1\|\omega\|^2\bar{\hat{u}} + k_{\text{on}}\bar{\hat{u}}] + \|\mathbf{v}_2(\omega)\|^2T_6[-k_{\text{off}}\bar{\hat{u}} + D_2\|\omega\|^2\bar{\hat{b}} + k_{\text{off}}\bar{\hat{b}}] - \\
& k_b\overline{I_{r_n}}[(T_6)^2 + (T_5)^2] + (k_{\text{off}}\hat{b} - k_{\text{on}}\hat{u})\|\mathbf{v}_2(\omega)\|^2T_8 - \\
& \|\omega\|^2[D_1(T_7)^2 + D_2(T_8)^2] + (k_{\text{on}}\hat{u} - k_{\text{off}}\hat{b})\|\mathbf{v}_2(\omega)\|^2T_7 + \\
& N^2\|\mathbf{v}_2(\omega)\|^4[-k_{\text{on}}\|u\|^2 + N^2k_{\text{off}}\overline{ub} + N^2k_{\text{on}}\overline{bu} - k_{\text{off}}\|b\|^2] - \\
& \|\omega\|^2\|\mathbf{v}_2(\omega)\|^2[D_1\hat{u}T_7 + D_2\hat{b}T_8] + k_b\|\mathbf{v}_2(\omega)\|^2[\widehat{\overline{I_{r_n}}b}T_6 + \widehat{\overline{I_{r_n}}u}T_5].
\end{aligned}
$$

A.2. Block Arnoldi, $\omega_1 = \omega_2 = 0$

The entries of M_1 from Section 3.3 are given by

$$
\begin{aligned}
M_1 &= X_1^H L X_1 \\
&= \begin{bmatrix} M_{11} & M_{12} \\ M_{21} & M_{22} \end{bmatrix}
\end{aligned}
$$

where

$$
\begin{aligned}
M_{11} &= -\overline{I_{r_n}}k_b \\
M_{12} &= \frac{-Nk_b(\overline{uI_{r_n}} + \overline{bI_{r_n}} + \overline{I_{r_n}}(\bar{u} + \bar{b}))}{\sqrt{2d_1}} \\
M_{21} &= \frac{N((k_{\text{off}} - k_{\text{on}})(\bar{u} - \bar{b}) - k_b(\overline{uI_{r_n}} + \overline{bI_{r_n}} + \overline{I_{r_n}}(\bar{u} + \bar{b})))}{\sqrt{2d_1}} \\
M_{22} &= \frac{n_1}{d_1}
\end{aligned}
$$

with

$$
\begin{aligned}
n_1 = {} & -k_bN^2\left(\overline{I_{r_n}u^2} + \overline{I_{r_n}b^2} - (\bar{u} + \bar{b})\overline{I_{r_n}u} - (\bar{u} + \bar{b})\overline{I_{r_n}b} + \overline{I_{r_n}}\left(\frac{\bar{u}^2}{2} + \frac{\bar{b}^2}{2} + \bar{u}\bar{b}\right)\right) - \\
& k_{\text{on}}\left(\|u\|^2 - N^2\bar{u}(\bar{u} + \bar{b}) + \frac{N^2(\bar{b} + \bar{u})^2}{4}\right) - k_{\text{off}}\left(\|b\|^2 - N^2\bar{b}(\bar{u} + \bar{b}) + \frac{N^2(\bar{b} + \bar{u})^2}{4}\right) + \\
& N^2(k_{\text{on}} + k_{\text{off}})\left(\overline{ub} - \frac{(\bar{b}^2 + \bar{u}^2)}{4} - \frac{\bar{b}\bar{u}}{2}\right) - (D_1\|\nabla u\|^2 + D_2\|\nabla b\|^2) \\
d_1 = {} & \|u\|^2 + \|b\|^2 - \frac{N^2(\bar{b} + \bar{u})^2}{2}.
\end{aligned}
$$

Similarly, the entries of $\tilde{M}_1$ from Section 3.3 are

$$
\begin{aligned}
\tilde{M}_1 &= \tilde{X}_1^H L \tilde{X}_1 \\
&= \begin{bmatrix} \tilde{M}_{11} & \tilde{M}_{12} \\ \tilde{M}_{21} & \tilde{M}_{22} \end{bmatrix}
\end{aligned}
$$

where

$$
\begin{aligned}
\tilde{M}_{11} &= -\overline{I_{r_n}}k_b - k_{\text{on}} - k_{\text{off}} \\
\tilde{M}_{12} &= \frac{k_bN(-k_{\text{on}}\overline{I_{r_n}u} + k_{\text{off}}\overline{I_{r_n}b} + \overline{I_{r_n}}(\bar{u}k_{\text{on}} - \bar{b}k_{\text{off}}))}{\sqrt{(k_{\text{on}}^2 + k_{\text{off}}^2)d_2}} \\
\tilde{M}_{21} &= \tilde{M}_{12} + \frac{N\left(\bar{u}\left(-k_{\text{off}}^2 + \frac{k_{\text{on}}k_{\text{off}}^3}{k_{\text{on}}^2 + k_{\text{off}}^2}\right) + \bar{b}\left(k_{\text{on}}^2 - \frac{k_{\text{on}}k_{\text{off}}^3}{k_{\text{on}}^2 + k_{\text{off}}^2}\right)\right)}{\sqrt{(k_{\text{on}}^2 + k_{\text{off}}^2)d_2}} \\
\tilde{M}_{22} &= \frac{n_2}{d_2}
\end{aligned}
$$

Please cite this article in press as: S. Sheikholeslami, J.V. Lambers, Modeling of first-order photobleaching kinetics using Krylov subspace spectral methods, Computers and Mathematics with Applications (2017), https://doi.org/10.1016/j.camwa.2017.10.019.

with

$$
\begin{aligned}
d_2 &= \|u\|^2 + \|b\|^2 - \frac{N^2\bar{u}^2k_{\text{on}}^2}{k_{\text{on}}^2+k_{\text{off}}^2} - \frac{N^2\bar{b}^2k_{\text{off}}^2}{k_{\text{on}}^2+k_{\text{off}}^2} + \frac{2N^2\bar{u}\bar{b}k_{\text{on}}k_{\text{off}}}{k_{\text{on}}^2+k_{\text{off}}^2}\\
n_2 &= -k_bN^2\left[\overline{I_{r_n}u^2} + \overline{I_{r_n}b^2} + \overline{I_{r_n}u}\left(\frac{2\bar{u}k_{\text{on}}^2}{k_{\text{on}}^2+k_{\text{off}}^2} - \frac{2\bar{b}k_{\text{off}}k_{\text{on}}}{k_{\text{on}}^2+k_{\text{off}}^2}\right) + \overline{I_{r_n}b}\left(\frac{-2\bar{u}k_{\text{on}}k_{\text{off}}}{k_{\text{on}}^2+k_{\text{off}}^2} + \frac{2\bar{b}k_{\text{off}}^2}{k_{\text{on}}^2+k_{\text{off}}^2}\right) + \right.\\
&\quad \left.\overline{I_{r_n}}\left(-\frac{\bar{u}^2k_{\text{on}}^2}{k_{\text{on}}^2+k_{\text{off}}^2} - \frac{\bar{b}^2k_{\text{off}}^2}{k_{\text{on}}^2+k_{\text{off}}^2} + \bar{u}\bar{b}\frac{2k_{\text{on}}k_{\text{off}}}{k_{\text{on}}^2+k_{\text{off}}^2}\right)\right] +\\
&\quad N^2(\overline{u\bar{b}}(k_{\text{on}}+k_{\text{off}}) + \bar{u}^2k_{\text{on}} + \bar{b}^2k_{\text{off}} - \bar{b}\bar{u}(k_{\text{on}}+k_{\text{off}})) -\\
&\quad (k_{\text{on}}\|u\|^2 + k_{\text{off}}\|b\|^2) - (D_1\|\nabla u\|^2 + D_2\|\nabla b\|^2).
\end{aligned}
$$

A.3. Approximate analytical solution, $\omega \neq 0$ case

The entries of M_1 and $\tilde{M}_1$ from Section 4.1 are given by

$$
\begin{aligned}
M_1 &= X_1^H L X_1\\
&= \begin{bmatrix} \dfrac{n_4}{u_{22}^2+k_{\text{off}}^2} & \dfrac{k_bk_{\text{off}}\widehat{I_{r_n}}(\overline{u_{22}}-k_{\text{on}})}{N^2\sqrt{u_{22}^2+k_{\text{off}}^2}\sqrt{k_{\text{on}}^2+k_{\text{off}}^2}} \\ \dfrac{k_bk_{\text{off}}\widehat{\overline{I_{r_n}}}(u_{22}-k_{\text{on}})}{N^2\sqrt{u_{22}^2+k_{\text{off}}^2}\sqrt{k_{\text{on}}^2+k_{\text{off}}^2}} & -k_b\overline{I_{r_n}} \end{bmatrix}\\
n_4 &= -k_b\overline{I_{r_n}}(u_{22}^2+k_{\text{off}}^2) - \|\omega\|^2(D_1u_{22}^2 + k_{\text{off}}^2D_2) -\\
&\quad (k_{\text{on}}u_{22}^2 + \overline{u_{22}}k_{\text{off}}^2 + k_{\text{off}}k_{\text{on}}u_{22} + k_{\text{off}}^3)\\
\tilde{M}_1 &= \tilde{X}_1^H L \tilde{X}_1\\
&= \begin{bmatrix} \dfrac{n_5}{u_{21}^2+k_{\text{off}}^2} & \dfrac{k_bk_{\text{off}}\widehat{I_{r_n}}(-\overline{u_{21}}+k_{\text{on}})}{N^2\sqrt{u_{21}^2+k_{\text{off}}^2}\sqrt{k_{\text{on}}^2+k_{\text{off}}^2}} \\ \dfrac{k_bk_{\text{off}}\widehat{\overline{I_{r_n}}}(-u_{21}+k_{\text{on}})}{N^2\sqrt{u_{21}^2+k_{\text{off}}^2}\sqrt{k_{\text{on}}^2+k_{\text{off}}^2}} & -k_b\overline{I_{r_n}} \end{bmatrix}\\
n_5 &= -k_b\overline{I_{r_n}}(u_{21}^2+k_{\text{off}}^2) - \|\omega\|^2(D_1u_{21}^2 + k_{\text{off}}^2D_2) -\\
&\quad (k_{\text{on}}u_{21}^2 + \overline{u_{21}}k_{\text{off}}^2 + k_{\text{off}}k_{\text{on}}u_{21} + k_{\text{off}}^3),
\end{aligned}
\tag{A.1}
$$

where $\bar{\hat{f}}$ is the complex conjugate of the discrete Fourier transform of the grid function f.

The eigenvalues of M_1 are

$$
\begin{aligned}
\lambda_{1,\omega} &= -\frac{1}{2(u_{22}^2+k_{\text{off}}^2)}(\|\omega\|^2(D_1u_{22}^2+k_{\text{off}}^2D_2)) - \frac{(k_{\text{on}}u_{22}^2 + \overline{u_{22}}k_{\text{off}}^2 + k_{\text{off}}k_{\text{on}}u_{22} + k_{\text{off}}^3)}{2(u_{22}^2+k_{\text{off}}^2)} -\\
&\quad k_b\overline{I_{r_n}} - \frac{1}{2}\left[\frac{1}{(u_{22}^2+k_{\text{off}}^2)^2}\|\omega\|^4(D_1u_{22}^2+k_{\text{off}}^2D_2)^2 + \right.\\
&\quad \frac{1}{(u_{22}^2+k_{\text{off}}^2)^2}(k_{\text{on}}u_{22}^2 + \overline{u_{22}}k_{\text{off}}^2 + k_{\text{off}}k_{\text{on}}u_{22} + k_{\text{off}}^3)^2 +\\
&\quad \frac{2}{(u_{22}^2+k_{\text{off}}^2)^2}\|\omega\|^2(D_1u_{22}^2+k_{\text{off}}^2D_2)(k_{\text{on}}u_{22}^2 + \overline{u_{22}}k_{\text{off}}^2 + k_{\text{off}}k_{\text{on}}u_{22} + k_{\text{off}}^3) +\\
&\quad \left.\frac{4k_b^2k_{\text{off}}^2\hat{I}_{r_n}^2(\overline{u}_{22}-k_{\text{on}})(u_{22}-k_{\text{on}})}{N^4(k_{\text{on}}^2+k_{\text{off}}^2)(k_{\text{off}}^2+u_{22}^2)}\right]^{1/2}\\
\lambda_{2,\omega} &= \frac{n_6}{d_6}
\end{aligned}
$$

where

$$
\begin{aligned}
d_6 = {} & \frac{-1}{u_{22}^2+k_{\text{off}}^2}\left[\|\omega\|^2(D_1u_{22}^2+k_{\text{off}}^2D_2)+(k_{\text{on}}u_{22}^2+\overline{u_{22}}k_{\text{off}}^2+k_{\text{off}}k_{\text{on}}u_{22}+k_{\text{off}}^3)\right]- \\
& 2k_b\overline{I_{r_n}}-\Bigg[\frac{1}{(u_{22}^2+k_{\text{off}}^2)^2}\|\omega\|^4(D_1u_{22}^2+k_{\text{off}}^2D_2)^2+ \\
& \frac{1}{(u_{22}^2+k_{\text{off}}^2)^2}(k_{\text{on}}u_{22}^2+\overline{u_{22}}k_{\text{off}}^2+k_{\text{off}}k_{\text{on}}u_{22}+k_{\text{off}}^3)^2+ \\
& \frac{2}{(u_{22}^2+k_{\text{off}}^2)^2}\|\omega\|^2(D_1u_{22}^2+k_{\text{off}}^2D_2)(k_{\text{on}}u_{22}^2+\overline{u_{22}}k_{\text{off}}^2+k_{\text{off}}k_{\text{on}}u_{22}+k_{\text{off}}^3)+ \\
& \frac{4k_b^2k_{\text{off}}^2\hat{I}_{r_n}^2(\overline{u}_{22}-k_{\text{on}})(u_{22}-k_{\text{on}})}{N^4(k_{\text{on}}^2+k_{\text{off}}^2)(k_{\text{off}}^2+u_{22}^2)}\Bigg]^{1/2} \\
n_6 = {} & \frac{2}{(u_{22}^2+k_{\text{off}}^2)}\left[k_b\overline{I_{r_n}}\|\omega\|^2(D_1u_{22}^2+k_{\text{off}}^2D_2)+k_b^2\overline{I_{r_n}}^2(u_{22}^2+k_{\text{off}}^2)+\right. \\
& \left.k_b\overline{I_{r_n}}(k_{\text{on}}u_{22}^2+\overline{u_{22}}k_{\text{off}}^2+k_{\text{off}}k_{\text{on}}u_{22}+k_{\text{off}}^3)\right]- \\
& \frac{2k_b^2k_{\text{off}}^2\hat{I}_{r_n}^2(\overline{u}_{22}-k_{\text{on}})(u_{22}-k_{\text{on}})}{N^4(k_{\text{on}}^2+k_{\text{off}}^2)(k_{\text{off}}^2+u_{22}^2)}.
\end{aligned}
\tag{A.2}
$$

Similarly, the eigenvalues of $\tilde{M}_1$ are

$$
\begin{aligned}
\tilde{\lambda}_{1,\omega} = {} & -\frac{1}{2(u_{21}^2+k_{\text{off}}^2)}(\|\omega\|^2(D_1u_{21}^2+k_{\text{off}}^2D_2))-\frac{(k_{\text{on}}u_{21}^2+\overline{u_{21}}k_{\text{off}}^2+k_{\text{off}}k_{\text{on}}u_{21}+k_{\text{off}}^3)}{2(u_{21}^2+k_{\text{off}}^2)}- \\
& k_b\overline{I_{r_n}}-\frac{1}{2}\Bigg[\frac{1}{(u_{21}^2+k_{\text{off}}^2)^2}\|\omega\|^4(D_1u_{21}^2+k_{\text{off}}^2D_2)^2+ \\
& \frac{1}{(u_{21}^2+k_{\text{off}}^2)^2}(k_{\text{on}}u_{21}^2+\overline{u_{21}}k_{\text{off}}^2+k_{\text{off}}k_{\text{on}}u_{21}+k_{\text{off}}^3)^2+ \\
& \frac{2}{(u_{21}^2+k_{\text{off}}^2)^2}\|\omega\|^2(D_1u_{21}^2+k_{\text{off}}^2D_2)(k_{\text{on}}u_{21}^2+\overline{u_{21}}k_{\text{off}}^2+k_{\text{off}}k_{\text{on}}u_{21}+k_{\text{off}}^3)+ \\
& \frac{4k_b^2k_{\text{off}}^2\hat{I}_{r_n}^2(-\overline{u}_{21}+k_{\text{on}})(-u_{21}+k_{\text{on}})}{N^4(k_{\text{on}}^2+k_{\text{off}}^2)(k_{\text{off}}^2+u_{21}^2)}\Bigg]^{1/2} \\
\tilde{\lambda}_{2,\omega} = {} & \frac{n_7}{d_7}
\end{aligned}
$$

where

$$
\begin{aligned}
d_7 = {} & \frac{-1}{u_{21}^2+k_{\text{off}}^2}\left[\|\omega\|^2(D_1u_{21}^2+k_{\text{off}}^2D_2)+(k_{\text{on}}u_{21}^2+\overline{u_{21}}k_{\text{off}}^2+k_{\text{off}}k_{\text{on}}u_{21}+k_{\text{off}}^3)\right]- \\
& 2k_b\overline{I_{r_n}}-\Bigg[\frac{1}{(u_{21}^2+k_{\text{off}}^2)^2}\|\omega\|^4(D_1u_{21}^2+k_{\text{off}}^2D_2)^2+ \\
& \frac{1}{(u_{21}^2+k_{\text{off}}^2)^2}(k_{\text{on}}u_{21}^2+\overline{u_{21}}k_{\text{off}}^2+k_{\text{off}}k_{\text{on}}u_{21}+k_{\text{off}}^3)^2+ \\
& \frac{2}{(u_{21}^2+k_{\text{off}}^2)^2}\|\omega\|^2(D_1u_{21}^2+k_{\text{off}}^2D_2)(k_{\text{on}}u_{21}^2+\overline{u_{21}}k_{\text{off}}^2+k_{\text{off}}k_{\text{on}}u_{21}+k_{\text{off}}^3)+ \\
& \frac{4k_b^2k_{\text{off}}^2\hat{I}_{r_n}^2(-\overline{u}_{21}+k_{\text{on}})(-u_{21}+k_{\text{on}})}{N^4(k_{\text{on}}^2+k_{\text{off}}^2)(k_{\text{off}}^2+u_{21}^2)}\Bigg]^{1/2} \\
n_7 = {} & \frac{2}{(u_{21}^2+k_{\text{off}}^2)}\left[k_b\overline{I_{r_n}}\|\omega\|^2(D_1u_{21}^2+k_{\text{off}}^2D_2)+k_b^2\overline{I_{r_n}}^2(u_{21}^2+k_{\text{off}}^2)+\right. \\
& \left.k_b\overline{I_{r_n}}(k_{\text{on}}u_{21}^2+\overline{u_{21}}k_{\text{off}}^2+k_{\text{off}}k_{\text{on}}u_{21}+k_{\text{off}}^3)\right]- \\
& \frac{2k_b^2k_{\text{off}}^2\hat{I}_{r_n}^2(-\overline{u}_{21}+k_{\text{on}})(-u_{21}+k_{\text{on}})}{N^4(k_{\text{on}}^2+k_{\text{off}}^2)(k_{\text{off}}^2+u_{21}^2)}.
\end{aligned}
$$

We note that $\hat{I}_{r_n}^2$ decays rapidly to zero at higher frequencies, so for such components it can be neglected for simplicity.

Please cite this article in press as: S. Sheikholeslami, J.V. Lambers, Modeling of first-order photobleaching kinetics using Krylov subspace spectral methods, Computers and Mathematics with Applications (2017), https://doi.org/10.1016/j.camwa.2017.10.019.

References

[1] U. Kubitscheck, Fluorescence Microscopy : From Principles to Biological Applications, Wiley-Blackwell, Weinheim, 2013. http://dx.doi.org/10.1002/9783527671595.
[2] K. Braeckmans, L. Peeters, N.N. Sanders, S. C. De Smedt, J. Demeester, Three-Dimensional fluorescence recovery after photobleaching with the confocal scanning laser microscope, Biophys. J. 85 (2003) 2240–2252.
[3] J. Braga, J.M.P. Desterro, M. Carmo-Fonseca, Intracellular macromolecular mobility measured by fluorescence recovery after photobleaching with confocal laser scanning microscopes, Mol. Biol. Cell 15 (2004) 4749.
[4] M. Kang, C.A. Day, E. DiBenedetto, A.K. Kenworthy, A quantitative approach to analyze binding diffusion kinetics by confocal FRAP, Biophys. J. 99 (2010) 2737–2747.
[5] M. Kang, C.A. Day, K. Drake, A.K. Kenworthy, E. DiBenedetto, A generalization of theory for two-dimensional fluorescence recovery after photobleaching applicable to confocal laser scanning microscopes, Biophys. J. 97 (2009) 1501–1511.
[6] K.S. Zadeh, H.J. Montas, A. Shirmohammadi, Identification of biomolecule mass transport and binding rate parameters in living cells by inverse modeling, BioMed Central Ltd. 3 (1) (2006) 36.
[7] J.V. Lambers, Enhancement of Krylov subspace spectral methods by Block Lanczos iteration, Electron. Trans. Numer. Anal. 31 (2008) 86–109.
[8] G.H. Golub, G. Meurant, Matrices, moments and quadrature, in: D.F. Griffiths, G.A. Watson (Eds.), Proceedings of the 15th Dundee Conference, June-July 1993, Longman Scientific and Technical, 1994.
[9] J.V. Lambers, An explicit, stable, high-order spectral method for the wave equation based on block Gaussian quadrature, IAENG J. Appl. Math. 38 (2008) 333–348.
[10] A. Cibotarica, J.V. Lambers, E.M. Palchak, Solution of nonlinear time-dependent PDEs through componentwise approximation of matrix functions, J. Comput. Phys. 321 (2016) 1120–1143.
[11] G.H. Golub, R. Underwood, The block Lanczos method for computing eigenvalues, in: Proceedings of a Symposium Conducted by the Mathematics Research Center, the University of Wisconsin–Madison, March 28–30, 1977, J. Rice Ed. Mathematical Software III, 1977, pp. 361–377.
[12] J.V. Lambers, A spectral time-domain method for computational electrodynamics, Adv. Appl. Math. Mech. 6 (2009) 781–798.
[13] D. Calvetti, S.-M. Kim, L. Reichel, Quadrature rules based on the Arnoldi process, SIAM J. Matrix Anal. 26 (2005) 765–781.
[14] Y. Saad, Numerical Methods for Large Eigenvalue Problems, Halsted Press, New York, 1992.
[15] G.H. Golub, C.F. Van Loan, Matrix Computations, third ed., The John Hopkins University Press, 1996.
[16] J.V. Lambers, Krylov subspace spectral methods for the time-dependent schr odinger equation with non-smooth potentials, Numer. Algorithms 51 (2009) 239–280.
[17] M. Kang, A.K. Kenworthy, A closed-form analytic expression for FRAP formula for the binding diffusion model, Biophys. J.: Biophys. Lett. 95 (2) (2008) L13–L15.
[18] B.L. Sprague, R.L. Pego, D.A. Stavreva, J.G. McNally, Analysis of binding reactions by fluorescence recovery after photobleaching, Biophys. J. 86 (2004) 3473–3495.
[19] S. Sheikholeslami, Solution of PDEs for First-Order Photobleaching Kinetics Using Krylov Subspace Spectral Methods, The University of Southern Mississippi, 2017 (Ph.D. thesis).
[20] M. Tokman, Efficient integration of large stiff systems of ODEs with exponential propagation iterative (EPI) methods, J. Comput. Phys. 213 (2006) 748–776.

Please cite this article in press as: S. Sheikholeslami, J.V. Lambers, Modeling of first-order photobleaching kinetics using Krylov subspace spectral methods, Computers and Mathematics with Applications (2017), https://doi.org/10.1016/j.camwa.2017.10.019.